Research Square

Preprints are preliminary reports that have not undergone peer review.
They should not be considered conclusive, used to inform clinical practice,
or referenced by the media as validated information.

Pattern-Guided Thermal Buckling and Shrinkage Simulation for Yarn-Level Woven Cloth

Jong-Hyun Kim

jonghyunkim@inha.ac.kr

Inha University

Article

Keywords:

Posted Date: July 7th, 2026

DOI: https://doi.org/10.21203/rs.3.rs-10159126/v1

License: This work is licensed under a Creative Commons Attribution 4.0 International License.
Read Full License

Additional Declarations: No competing interests reported.

Version of Record: A version of this preprint was published at Scientific Reports on September 26th, 2026. See the published version at https://doi.org/10.1038/s41598-026-71779-6.

Pattern-Guided Thermal Buckling and Shrinkage Simulation for Yarn-Level Woven Cloth

Jong-Hyun Kim[1]

[1]College of Software and Convergence (Department of Artificial Intelligence, Design Technology), Graduate School of Electrical and Computer Engineering, Inha University, Michuhol-gu, Incheon 22212, South Korea
[*]corresponding author: jonghyunkim@inha.ac.kr

ABSTRACT

Woven cloth exhibits complex deformation behavior due to yarn-level interlacing structures, directional tension transfer, and the thermal response of fiber materials. In particular, when localized heat is applied, cloth does not simply shrink uniformly over its surface; instead, it forms pattern-dependent shrinkage directions, twisting, thermal softening, and out-of-plane buckling wrinkles. However, existing cloth simulation methods often treat heat-induced deformation as surface-level shrinkage or uniform material variation, making it difficult to represent pattern-dependent thermal buckling phenomena arising from yarn-level woven structures. This paper proposes a yarn-level thermal shrinkage and buckling wrinkle simulation method that accounts for woven patterns. The proposed method represents the cloth using a woven structure composed of warp and weft yarns, computes directional heat diffusion along yarn edges, and applies temperature-dependent temporary shrinkage, permanent shrinkage, and thermal softening to each yarn segment. In addition, by using the over-under relationship of the weave pattern and spatial differences in shrinkage, the method computes a shrinkage-gradient-based thermal buckling force, thereby inducing localized lifting, folding, and nonuniform wrinkle formation in heated regions rather than simple planar contraction. To this end, the thermal shrinkage amount of each node is estimated, the buckling strength is derived from shrinkage differences with neighboring nodes, and both pattern-dependent crossing directions and fine yarn-level irregularities are incorporated. Experimental results with various weave patterns show that the proposed method can generate different shrinkage and wrinkle behaviors under the same thermal conditions depending on patterns such as plain, basket, twill, satin, checker, and herringbone weaves. Compared with applying thermal shrinkage alone, the proposed pattern-guided thermal buckling model more effectively represents nonuniform shrinkage boundaries, localized out-of-plane wrinkles, and yarn-direction-dependent shape variations observed in thermally deformed fabrics. This study provides a simulation-based framework for visually analyzing and controlling heat-induced woven-cloth deformation at the yarn level, and it can be applied to digital textile design, physically based fabric deformation visualization, and virtual garment production.

Introduction

Woven cloth has a fine-scale structure formed by repeated interlacing of warp and weft yarns. This structure directly affects not only the visual appearance of cloth but also tension transfer, bending resistance, friction, shrinkage anisotropy, and wrinkle formation. In particular, when localized heat is applied, cloth does not simply undergo uniform area shrinkage. In real fabrics, heated yarns contract more strongly than the surrounding region, and the resulting shrinkage differences, together with constraints from the interlacing structure, produce localized lifting, folding, twisting, and out-of-plane buckling wrinkles.

Figure 1 intuitively illustrates the problem addressed in this study. When a localized heat source is applied to a yarn-level woven structure, the yarns in the high-temperature region shrink more strongly and become softer than those in the surrounding region. During this process, the deformation does not remain as simple planar shrinkage, but develops into localized out-of-plane deformation and buckling wrinkles under the influence of the warp–weft crossing structure and weave pattern. Therefore, representing heat-induced deformation of woven cloth requires a model that considers yarn-level structure and pattern information, rather than a surface-level uniform shrinkage model.

Existing cloth simulation methods have mainly used continuous surface meshes or particle-based models to handle large-scale garment deformation, collision, wrinkles, and friction. These methods are effective for efficiently representing macroscopic cloth motion, but they have limitations in directly capturing pattern-dependent deformation that arises at the yarn level. In particular, when dealing with heat-induced deformation, many approaches approximate shrinkage through temperature-dependent material coefficients or surface scaling. However, in real woven cloth, heat diffuses anisotropically along the yarn connectivity, the degrees of shrinkage differ between the warp and weft directions, and compression accumulates locally due to the interlacing structure. To represent these phenomena, it is necessary to consider not only simple length reduction but also yarn-level shrinkage nonuniformity and the buckling mechanism.

Yarn-level cloth simulation is well suited for representing fine-scale deformation caused by woven structures because it

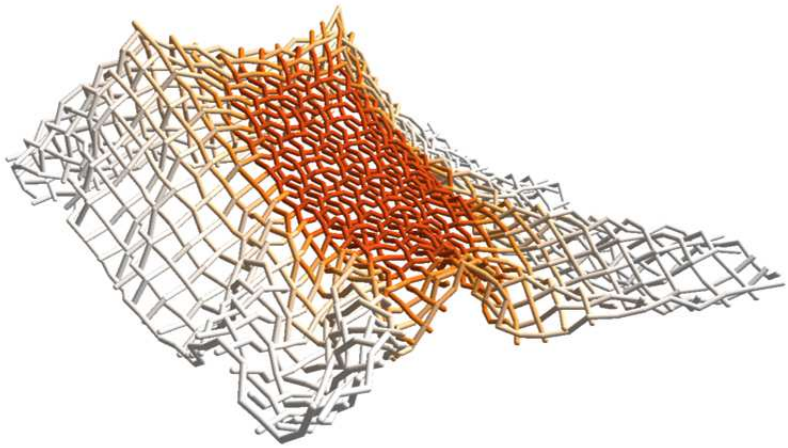


Figure 1. Overview of the proposed pattern-guided thermal shrinkage and buckling simulation for yarn-level woven cloth. A localized heat source raises the temperature of selected yarn regions, causing anisotropic shrinkage, thermal softening, twisting, and out-of-plane buckling. The color distribution represents the temperature-induced response, where hotter yarn regions undergo stronger shrinkage and wrinkle formation.

directly handles the positions and interactions of individual yarns. However, existing yarn-level models have mainly focused on elastic deformation, contact, friction, sliding, and the geometric construction of weave patterns. In contrast, relatively little work has integrated heat-induced yarn shrinkage, thermal softening, directional shrinkage differences, and pattern-dependent buckling wrinkles. A key issue in thermal deformation is that the heated region does not merely become shorter; rather, shrinkage differences between heated and surrounding yarns create compressive instability. This buckling depends on the over-under relationship of the weave pattern and the yarn directions, so pattern information must be explicitly incorporated into the deformation model.

This paper proposes a yarn-level thermal shrinkage and buckling simulation method that accounts for woven patterns. The proposed method represents regular woven cloth as a network of warp and weft yarns, and computes heat diffusion, temperature-dependent shrinkage, thermal softening, wrinkle forces, and pattern-guided buckling forces along each yarn segment. Heat diffusion is treated anisotropically by assigning different diffusion coefficients to the warp and weft directions, while temperature changes induce temporary and permanent shrinkage in each yarn segment. In addition, in high-temperature regions, the stretch response of yarn segments is weakened to produce to allow heated yarns to deform more easily, and a normal-direction buckling force is generated using shrinkage differences and pattern information.

The core idea of the proposed method is to convert spatial differences in thermal shrinkage into out-of-plane buckling. At each node, a temperature-dependent shrinkage amount is estimated, and a local shrinkage gradient is obtained by comparing it with the shrinkage values of neighboring nodes. Regions that shrink more strongly than their surroundings are considered locations where compression accumulates, and this value is converted into a normal-direction buckling force. In addition, the over-under relationship of the weave pattern is used to control the direction and strength of buckling, allowing different wrinkle behaviors to emerge under the same thermal condition depending on the pattern. Fine yarn-level irregularities are also incorporated to more naturally represent irregular wrinkles and nonuniform shrinkage boundaries observed in thermally deformed fabrics.

The main contributions of this study are as follows.

- We propose a yarn-level thermal shrinkage and buckling simulation framework that incorporates the over-under structure of woven patterns.
- We combine anisotropic heat diffusion along warp and weft yarn directions with temperature-dependent temporary and permanent shrinkage models.
- We model thermal softening by weakening the stretch response of yarn segments in high-temperature regions and by generating deformation through shrinkage-driven wrinkle and buckling forces.
- We introduce a pattern-guided thermal buckling force that uses spatial shrinkage differences and weave-pattern information to generate localized out-of-plane wrinkles rather than planar shrinkage.

- We compare pattern-dependent shrinkage and wrinkle behavior under thermal conditions across various weave patterns, including plain, basket, twill, satin, checker, and herringbone structures.

Experimental results show that the proposed method generates richer deformation behavior than a simple thermal shrinkage model. In particular, by applying a buckling force based on shrinkage differences, irregular wrinkles, localized lifting, and pattern-directional deformation emerge around heated regions. This work provides a foundation for simulating and analyzing heat-induced woven-cloth deformation based on fine-scale yarn structures, and it can be applied to digital textile design, physically based fabric deformation visualization, and virtual garment production.

Problem Statement

The objective of this study is to simulate yarn-level shrinkage, thermal softening, and pattern-dependent buckling wrinkles caused by localized thermal input. To this end, woven cloth is represented not as a simple continuous surface, but as a yarn network in which warp and weft yarns intersect. Because the over-under relationship at each crossing affects compression transfer and the direction of out-of-plane deformation after thermal shrinkage, this relationship is explicitly modeled using a pattern function P.

The problem addressed in this paper can be defined as follows. The inputs are a weave pattern P, an initial yarn-level cloth configuration $\mathscr{Y}^0$, a heat-source position $\mathbf{h}$, a heat-source radius r_h, a heat-source temperature T_h, and a set of material parameters Θ. Here, $\mathscr{Y}$ consists of yarn nodes and yarn segments, and each node stores its position $\mathbf{x}_i$, velocity $\mathbf{v}_i$, temperature T_i, shrinkage amount s_i, and thermal softening state. The goal is to compute the deformed yarn configuration $\mathscr{Y}^{t+\Delta t}$ at the next time step from the time-varying temperature field T^t and yarn state $\mathscr{Y}^t$.

The proposed model must satisfy three requirements. First, heat should not diffuse uniformly over the entire cloth surface, but should propagate along the yarn connectivity. Since the material properties and connectivity structures of the warp and weft directions may differ, heat diffusion must be directional. Second, heat-induced shrinkage should be represented not as global surface scaling, but as changes in the rest length of each yarn segment. This produces length and tension differences between heated and unheated yarns. Third, these shrinkage differences should be combined with the over-under structure of the weave pattern and converted into a normal-direction buckling force. In other words, the central problem of this study is not simply to treat thermal shrinkage as length reduction, but to determine the direction and strength of wrinkle formation using spatial shrinkage differences and weave-pattern information.

The outputs are the updated yarn positions, temperature distribution, temporary and permanent shrinkage, and buckling wrinkle shapes at each time step. In particular, even under the same heat source and material parameters, the final deformation should vary depending on weave patterns such as plain, basket, twill, satin, and herringbone structures. In a plain weave, the dense crossing structure may produce relatively uniform and fine wrinkles, whereas basket or satin patterns may produce broader shrinkage regions or smoother shrinkage boundaries due to block structures or long yarn floats. In twill and herringbone patterns, the diagonal over-under structure can influence the directionality of buckling.

Therefore, the goal of this study is not merely to simulate "cloth that shrinks under heat," but to generate 'thermal buckling wrinkles induced by weave patterns." To achieve this, the proposed method combines yarn-edge-based anisotropic heat diffusion, temperature-dependent temporary and permanent shrinkage, thermal softening, shrinkage-driven wrinkle forces, and pattern-guided buckling forces to compute yarn-level thermal deformation.

Related Work

Yarn-Level Cloth Simulation

Cloth simulation has traditionally been modeled at the surface or shell level, where fabric is represented as a continuous thin sheet. Such models are efficient and effective for large-scale garment motion, but they do not explicitly describe the internal yarn structure that governs many characteristic behaviors of woven and knitted textiles. In particular, anisotropic stiffness, local compression, inter-yarn friction, yarn slippage, and pattern-dependent deformation are difficult to reproduce when fabric is treated as a homogeneous sheet. To address this limitation, yarn-level cloth simulation has been studied as a way to represent fabric mechanics through the motion and contact of individual yarns.

Kaldor et al.[1] introduced one of the earliest yarn-level models for knitted cloth, representing yarns as deformable curves rather than treating fabric as a sheet. Their method demonstrated that the nonlinear deformation of knitted fabrics can emerge from loop-level yarn geometry. They later improved the efficiency of yarn-based simulation by reducing the cost of yarn–yarn contact handling through adaptive contact linearization[2]. These works established the importance of explicitly modeling yarn interactions, but their focus was mainly on knitted structures and dynamic deformation under mechanical loading, rather than thermally induced shrinkage or shrinkage-driven wrinkling.

For woven fabrics, Cirio et al.[3] proposed an efficient yarn-level simulation method based on interlaced yarn discretization. Their model captures the macroscopic behavior of woven cloth from yarn properties, weave patterns, and frictional contact

between yarns. Cirio et al.[4] further introduced sliding persistent contacts, allowing yarn–yarn contact to be treated persistently while still permitting sliding. This significantly improved the practicality of yarn-level cloth simulation by avoiding repeated expensive contact detection. These approaches are highly relevant to the present work because they show that woven-cloth deformation is strongly affected by inter-yarn constraints and friction. However, their main target is mechanical draping and contact-driven deformation, whereas our work focuses on thermal shrinkage and the resulting buckling and wrinkle formation in yarn-level woven structures.

Yarn-level modeling has also been studied from an authoring and design perspective. Leaf et al.[5] proposed an interactive system for designing periodic yarn-level cloth patterns, enabling users to author and simulate knitted and woven structures. This line of work is important because it connects yarn topology and fabric pattern to the resulting mechanical behavior. However, such authoring-oriented systems are not designed to simulate thermal contraction, yarn shortening, or heat-induced wrinkle evolution.

Hybrid and Homogenized Models for Yarn-Level Effects

Although yarn-level simulation provides high fidelity, directly simulating every yarn in a garment is computationally expensive. To overcome this issue, several studies have investigated hybrid or homogenized models that approximate yarn-level behavior at a coarser scale. Casafranca et al.[6] proposed a hybrid representation that combines yarns and triangles in cloth simulation. Their method uses a triangle-based model for most of the garment while applying yarn-level models only in selected regions where detailed yarn behavior is important. This strategy is useful for reducing computational cost while retaining local yarn-level effects. However, yarn thermal shrinkage and its propagation into structured wrinkle patterns are not the main focus of their work.

Sperl et al.[7] introduced homogenized yarn-level cloth, where many yarn-level simulations are used to construct a constitutive model for a thin-shell solver. This method captures the macroscopic effect of yarn-level patterns while avoiding the cost of full yarn-level simulation. Sperl et al.[8] further proposed mechanics-aware deformation of yarn pattern geometry, where yarn-level geometric details are animated on top of a deforming cloth surface. Their work bridges the gap between shell-level simulation and yarn-level appearance. Sperl et al.[9] also estimated yarn-level simulation models for production fabrics from measured fabric responses, showing that real textile measurements can be connected to yarn-level mechanical parameters.

Recent studies further extend this direction using differentiable simulation and neural models. Gong et al.[10] proposed a fine-grained differentiable yarn-level model for fabrics, enabling gradient-based learning of yarn-level parameters and interactions. Feng et al.[11] introduced neural-assisted homogenization of yarn-level cloth, using neural networks to improve the stability and efficiency of homogenized yarn-level constitutive models. Zhang et al.[12] estimated shell-level elasticity parameters from homogenized yarn-level models, allowing real fabrics to be represented through efficient shell simulations while preserving nonlinear and anisotropic behavior originating from yarn structures. Yuan et al.[13] proposed volumetric homogenization for knitwear simulation, showing that spatially varying homogenization can better capture complex knitted patterns than a single global material model.

These studies indicate that yarn-level mechanics are necessary for representing fabric-specific deformation, but they also highlight the computational difficulty of directly resolving all yarn interactions. In contrast, our work focuses on a different but complementary problem: how thermal contraction at the yarn level produces pattern-dependent buckling and wrinkles in woven cloth. Rather than only transferring yarn-level mechanics to a shell model, the proposed method explicitly uses weave-pattern information and shrinkage behavior to generate thermally induced wrinkle structures.

Wrinkle Formation and Persistent Cloth Deformation

Wrinkle simulation has been widely studied in computer graphics because wrinkles are essential for visual realism. Bridson et al.[14] presented important techniques for simulating clothing with folds and wrinkles, emphasizing robust collision handling and visually rich garment deformation. Rohmer et al.[15] proposed a procedural method for augmenting coarse cloth simulations with realistic-looking animated wrinkles by analyzing compression directions in the coarse simulation. M"uller and Chentanez[16] introduced wrinkle meshes, which attach high-resolution wrinkle details to coarse dynamic meshes. These methods can efficiently enrich visual detail, but the generated wrinkles are usually controlled by surface-level compression or procedural rules rather than by explicit yarn contraction.

Data-driven wrinkle synthesis has also been explored. L"ahner et al.[17] proposed DeepWrinkles, which reconstructs high-frequency clothing wrinkle details from captured data. Chen et al.[18] proposed a multi-feature super-resolution network for synthesizing high-resolution cloth wrinkles from low-resolution simulations. These methods can generate visually convincing wrinkles, but they rely on training data and generally do not model the physical mechanism of yarn shrinkage or thermal buckling.

Another important direction is persistent wrinkle modeling. Miguel et al.[19] modeled internal friction in cloth and showed that hysteresis plays an important role in repeated wrinkle formation. Gong et al.[20] recently proposed a cloth simulator for time-dependent persistent wrinkles, modeling the interaction between internal friction and plasticity. Their work is highly

Pattern	Structural characteristic	Expected deformation under thermal shrinkage
Plain weave	Repeated 1-over/1-under interlacing	Dense and relatively uniform fine wrinkle formation
Basket weave	Multiple yarns interlace in block-wise units	Block-wise shrinkage and formation of broad wrinkle patches
Twill weave	Diagonal float structure	Wrinkles aligned along the diagonal yarn direction
Satin weave	Long yarn floats	Smoother surface contraction with reduced wrinkle frequency
Rib weave	Different warp/weft yarn radii and densities	Strongly directional stripe-like deformation
Checker weave	Block-wise inversion of the weave pattern	Alternating wrinkle intensity depending on spatial location
Waffle/Honeycomb	Cell-like or cavity-like structure	Enhanced local buckling near cell boundaries
Seersucker/Wave weave	Initial wave-like or stripe-like structure	Periodic wrinkles emphasized by thermal shrinkage

Table 1. Representative weave patterns used in the proposed yarn-level thermal shrinkage simulation.

relevant because persistent wrinkles in real fabrics often depend on deformation history. However, their model primarily focuses on time-dependent wrinkle persistence under mechanical deformation, whereas our work studies wrinkles generated by thermal shrinkage and yarn-level buckling. Therefore, the proposed method complements persistent wrinkle models by addressing a different source of wrinkle formation: thermally induced contraction of yarns in structured woven patterns.

Thermal Shrinkage and Environmentally Induced Deformation

Thermal and environmental stimuli can significantly change the shape of thin materials. Chen et al.[21] presented a physically based thin-shell model for environmentally induced deformation, including effects caused by heat, moisture, and growth. Their formulation demonstrates that changes in the rest metric or rest curvature of a thin shell can produce large deformations such as curling and bending. Jeong et al.[22] simulated shrinkage, wrinkling, and ablation of burning cloth and paper by combining heat transfer, shrinkage, and partial ablation in a thin-shell framework. This work is closely related to our topic because it explicitly links heat-induced shrinkage to wrinkling. However, the material is modeled as a shell structure, and the internal yarn arrangement of woven cloth is not explicitly considered.

Textile engineering studies have also analyzed shrinkage at the yarn and fabric levels. Perera and Lanarolle[23] investigated the thermal shrinkage behavior of polyester yarns and plain knitted fabrics, showing that thermal processes can change fabric dimensions through both yarn shrinkage and structural changes in the fabric. Ahirwar and Behera[24] proposed a machine-learning-based model to predict the shrinkage behavior of stretch fabrics, while Ahmad et al.[25] analyzed how core-spun yarn characteristics affect shrinkage and stretch behavior in woven fabrics. These studies provide useful experimental evidence that yarn composition, yarn structure, and heat-treatment conditions strongly influence fabric shrinkage. However, they mainly focus on measurement, prediction, or textile manufacturing analysis, not on dynamic graphical simulation of shrinkage-induced wrinkles.

Compared with these studies, our method aims to connect textile-level shrinkage behavior with computer-graphics-oriented yarn-level simulation. Specifically, the proposed approach treats shrinkage not as uniform scaling of the cloth surface, but as pattern-aware contraction of yarns. This formulation is necessary because woven cloth does not contract as a homogeneous sheet under localized heating. When warp and weft yarns contract under thermal stimuli, local constraints at yarn crossings induce compression, bending, and buckling. These effects can produce wrinkles that are aligned with or constrained by the weave pattern. Therefore, the proposed method targets a phenomenon that is not fully addressed by previous shell-level shrinkage models, procedural wrinkle synthesis, or general yarn-level mechanical simulation.

Positioning of the Proposed Method

Existing yarn-level methods successfully reproduce detailed fabric mechanics by modeling yarn motion, contact, friction, and sliding. Homogenization methods accelerate these effects by transferring yarn-level responses to shell-level simulations. Wrinkle synthesis methods generate visually detailed folds and high-frequency surface deformations, while textile studies analyze how heat treatment and yarn properties affect fabric shrinkage. However, these research directions are still weakly connected in the context of thermal shrinkage and wrinkle generation for yarn-level woven cloth.

Our work addresses this gap by using yarn-level shrinkage as the driving mechanism for thermally induced buckling in woven structures. The resulting deformation is not limited to simple length reduction; instead, shrinkage generates local compression, buckling, and wrinkle patterns through yarn-level constraints. In this sense, our work differs from prior yarn-level simulation by introducing thermal shrinkage as a driving mechanism, differs from shell-level shrinkage models by explicitly considering woven yarn structure, and differs from procedural or data-driven wrinkle synthesis by deriving wrinkle formation from yarn-level contraction and weave-pattern constraints.

Module	Main variables	Role in the simulation
Yarn-level structure	$\mathbf{x}_{i,j}$, $(u_{i,j}, v_{i,j})$, $P(i,j)$	Represents woven cloth as intersecting warp and weft yarns with pattern-dependent over-under relationships.
Heat diffusion	$T_{i,j}$, k_{warp}, k_{weft}, $Q_{i,j}$	Propagates heat along yarn edges and generates anisotropic temperature distributions.
Temporary shrinkage	s^{u}_{temp}, s^{v}_{temp}	Produces immediate temperature-dependent yarn contraction in warp and weft directions.
Permanent shrinkage	$s_{\text{perm},u}$, $s_{\text{perm},v}$, h_p	Accumulates residual shrinkage when the yarn is exposed to high temperature.
Contracted rest length	ℓ_0, $\tilde{s}$, ℓ_T	Converts thermal shrinkage into shortened yarn segment rest lengths.
Thermal softening	γ_T, k_s	Reduces stretch stiffness in heated regions, allowing easier deformation.
Wrinkle force	$a_{i,j}$, $\phi_{i,j}$, $\mathbf{f}^{\text{wrinkle}}_{i,j}$	Generates local normal-direction wrinkle perturbations from directional shrinkage differences.
Buckling force	$\Delta_s(i,j)$, $P(i,j)$, $\mathbf{f}^{\text{buckling}}_{i,j}$	Produces pattern-guided out-of-plane buckling from spatial shrinkage differences.
Twisting force	τ_j, $\mathbf{s}_j$, $\mathbf{f}^{\text{twist}}_{j}$	Adds yarn-directional twisting deformation caused by anisotropic shrinkage.
Time integration	$\mathbf{x}^{t+\Delta t}$, $\mathbf{v}^{t+\Delta t}$, $u^{t+\Delta t}$, $v^{t+\Delta t}$	Updates physical positions and parametric coordinates using Verlet integration.

Table 2. Summary of the main algorithmic modules and their roles in the proposed yarn-level thermal shrinkage simulation.

Algorithm

This section describes the proposed *pattern-guided thermal shrinkage and wrinkle simulation* algorithm. The proposed method does not interpret woven cloth only as a continuous cloth surface, but instead models it as a yarn-level structure composed of warp and weft yarns. Each yarn segment decreases its rest length according to temperature, and the difference in shrinkage between the warp and weft directions, the directionality of heat diffusion, and the over-under structure of the weave pattern together generate local compression, buckling, wrinkles, and twisting deformation.

Table 2 summarizes how the proposed method is organized into thermal, mechanical, and pattern-guided deformation modules. The first group of modules updates the temperature field and converts it into temporary and permanent shrinkage. The second group converts shrinkage into contracted yarn rest lengths and thermally softened stretch forces. The final group adds wrinkle, buckling, and twisting forces before the node states are advanced through time integration.

Yarn-Level Woven Cloth Representation

The woven cloth is represented as a yarn grid of size $W \times H$. Each grid node corresponds to an intersection between a warp yarn and a weft yarn, and the three-dimensional position of node (i,j) is defined as

$$\mathbf{x}_{i,j} \in \mathbb{R}^3, \tag{1}$$

where i and j denote the row and column indices, respectively. Each node stores its position $\mathbf{x}_{i,j}$, velocity $\mathbf{v}_{i,j}$, normal vector $\mathbf{n}_{i,j}$, parametric coordinate $(u_{i,j}, v_{i,j})$, temperature $T_{i,j}$, permanent shrinkage, and twisting state.

The initial parametric coordinates are defined as

$$u_{i,j} = \frac{j}{W-1}, \qquad v_{i,j} = \frac{i}{H-1}. \tag{2}$$

Using these coordinates, the initial positions are placed on a rectangular cloth domain as

$$\mathbf{x}^0_{i,j} = \left[\left(v_{i,j} - \frac{1}{2} \right) L_x,\ 0,\ \left(u_{i,j} - \frac{1}{2} \right) L_z \right]^T, \tag{3}$$

where L_x and L_z denote the cloth size in the row and column directions, respectively.

In the proposed method, yarns in the row direction are defined as warp strands, while yarns in the column direction are defined as weft strands. Each strand consists of a set of yarn segments connecting adjacent nodes, and each segment has a rest length that changes according to temperature. Therefore, the proposed representation can directly reflect the shortening of yarns caused by heat.

Pattern Function for Woven Structure

The over-under relationship of the woven structure is defined using a pattern function:

$$P(i,j) = \begin{cases} +1, & \text{if the warp yarn passes over the weft yarn,} \\ -1, & \text{if the weft yarn passes over the warp yarn.} \end{cases} \tag{4}$$

This function is used to represent various weave patterns, including plain weave, basket weave, twill, satin, rib, checker, waffle, herringbone, diamond twill, honeycomb, seersucker, jacquard block, and wave weave. In this study, the pattern function is not used only for rendering the over-under arrangement, but also for determining the direction of out-of-plane buckling caused by thermal shrinkage. In other words, even when the same temperature field and shrinkage rate are applied, the direction and distribution of wrinkles vary depending on the weave pattern.

Table 1 summarizes the representative weave patterns used in this study, their structural characteristics, and the expected deformation behavior under thermal shrinkage. In particular, plain weave, which has dense crossings, tends to form relatively uniform fine wrinkles, whereas twill and herringbone patterns generate directional wrinkles due to their yarn floats and diagonal structures. In addition, patterns with spatially repeated structures, such as waffle, honeycomb, and seersucker, induce more pronounced local buckling because thermal shrinkage is concentrated along specific cell boundaries or stripe directions.

These pattern-dependent differences are later reflected in the computation of the thermal buckling force through the pattern sign $P(i,j)$. Therefore, the proposed method does not simply add surface wrinkles using arbitrary noise, but generates pattern-aware wrinkles by jointly considering the over-under structure of the weave pattern and the local compression caused by thermal shrinkage.

Anisotropic Heat Diffusion along Yarn Edges

Heat does not diffuse uniformly over the entire cloth surface; instead, it propagates along yarn segments. When two adjacent nodes a and b are connected by a yarn segment, the heat flow between them is computed as

$$q_{a\to b} = k_d \left(T_b - T_a\right), \tag{5}$$

where T_a and T_b are the current temperatures of the two nodes, and k_d is the heat diffusion coefficient. In the proposed method, different heat diffusion rates are assigned to the warp and weft directions:

$$k_d = \begin{cases} k_{\text{warp}}, & \text{warp yarn segment,} \\ k_{\text{weft}}, & \text{weft yarn segment.} \end{cases} \tag{6}$$

This directional heat diffusion allows heat to propagate faster along one direction, thereby inducing nonuniform shrinkage and wrinkle formation in the warp and weft directions.

The heat source is applied to a circular region centered at a specific position $\mathbf{c}_h = (c_x, c_z)$ on the cloth. When a node $\mathbf{x}_{i,j}$ lies within the heat-source radius r_h, the heat-source term is defined as

$$Q_{i,j} = \lambda_h \exp\left(-\frac{\left|\mathbf{x}_{i,j}^{xz} - \mathbf{c}_h\right|^2}{r_h^2}\right)\left(T_h - T_{i,j}\right), \tag{7}$$

where $\mathbf{x}_{i,j}^{xz}$ is the position of the node on the xz plane, T_h is the heat-source temperature, and λ_h is the heat-source strength.

Cooling in air is computed using a linear damping term that returns the temperature to the rest temperature T_0:

$$C_{i,j} = -k_c \left(T_{i,j} - T_0\right), \tag{8}$$

where k_c is the air cooling coefficient. The final temperature is updated explicitly as

$$T_{i,j}^{t+\Delta t} = \text{clamp}\left(T_{i,j}^{t} + \Delta t \left(\Delta T_{i,j} + Q_{i,j} + C_{i,j}\right), T_0,\ T_h\right). \tag{9}$$

Figure 2 shows the yarn-edge-based anisotropic heat diffusion result used in the proposed method. In the figure, red and yellow regions indicate yarn regions with relatively high temperatures, while blue regions indicate low-temperature regions where heat has not sufficiently propagated. In the proposed method, heat is not uniformly diffused across the entire cloth surface, but is transmitted along warp and weft yarn segments. In addition, because different heat diffusion coefficients are applied to the warp and weft directions, the temperature field does not spread simply in a circular manner, but expands anisotropically according to the yarn directions and woven structure.

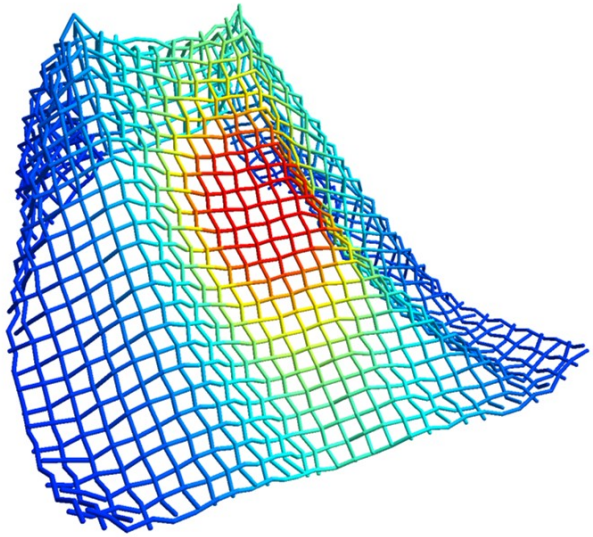


Figure 2. Anisotropic heat diffusion result on the yarn-level woven cloth. The color distribution represents the propagated temperature field along the yarn network, where red and yellow indicate higher temperature regions and blue indicates lower temperature regions. Because heat diffusion is computed along warp and weft yarn edges with different diffusion coefficients, the temperature field spreads directionally rather than uniformly over the cloth surface.

This anisotropic heat diffusion directly affects subsequent thermal shrinkage and buckling deformation. In high-temperature regions, the yarn rest length decreases more strongly and the stretch stiffness is reduced, allowing those regions to shrink faster and deform more easily than their surroundings. In contrast, surrounding regions with weaker heat propagation relatively preserve their original structure, producing shrinkage differences between heated and unheated regions. These differences are interpreted as local compression through the shrinkage Laplacian and ultimately generate a pattern-guided buckling force in the normal direction. Therefore, Figure 2 visually illustrates how heat diffusion, directional shrinkage, and out-of-plane buckling are connected in the proposed method.

Temperature-Dependent Temporary Shrinkage

The temporary shrinkage that occurs immediately due to the current temperature is computed as

$$s_{\text{temp}}(T) = \text{clamp}\left(\alpha_s\left(T - T_0\right), 0,\ s_{\text{temp}}^{\max}\right). \tag{10}$$

Here, α_s is the temperature-dependent shrinkage coefficient, and $s_{\text{temp}}^{\max}$ is the maximum temporary shrinkage ratio. In the proposed method, the shrinkage rates in the warp and weft directions are separated as

$$s_{\text{temp}}^{u} = \text{clamp}\left(\alpha_u\left(T - T_0\right), 0,\ s_{\text{temp}}^{\max}\right), \tag{11}$$

$$s_{\text{temp}}^{v} = \text{clamp}\left(\alpha_v\left(T - T_0\right), 0,\ s_{\text{temp}}^{\max}\right). \tag{12}$$

When $\alpha_u > \alpha_v$, the warp direction shrinks faster than the weft direction, and this difference becomes a major source of directional wrinkles.

Accumulation of Permanent Shrinkage

A yarn exposed to high temperature for a certain period does not fully recover its original length even after cooling. To represent this behavior, permanent shrinkage is accumulated only when the temperature exceeds the threshold T_p. The heat activation factor is defined as

$$h_p = \text{clamp}\left(\frac{T_{i,j} - T_p}{T_h - T_p}, 0,\ 1\right). \tag{13}$$

The permanent shrinkage values in the warp and weft directions are updated as

$$s_{\text{perm},u}^{t+\Delta t} = \text{clamp}\left(s_{\text{perm},u}^{t} + r_p h_p, 0,\ s_{\text{perm}}^{\max}\right), \tag{14}$$

$$s_{\text{perm},v}^{t+\Delta t} = \text{clamp}\left(s_{\text{perm},v}^{t} + 0.65 r_p h_p, 0,\ s_{\text{perm}}^{\max}\right). \tag{15}$$

Here, r_p is the permanent shrinkage rate. The coefficient 0.65 makes the accumulated permanent shrinkage in the weft direction smaller than that in the warp direction, preserving directional shrinkage differences even after thermal exposure.

Thermally Contracted Yarn Rest Length

The rest length of each yarn segment is updated every frame according to the current temperature and the accumulated permanent shrinkage. The original length of a warp segment is computed as

$$\ell_0^u = L_{\text{warp}}\left(u_b - u_a\right), \tag{16}$$

and the original length of a weft segment is computed as

$$\ell_0^v = L_{\text{weft}}\left(v_b - v_a\right). \tag{17}$$

Given the average temperature $\bar{T}$ of a yarn segment consisting of two nodes a and b, the total shrinkage ratio of the segment is defined as

$$s = s_{\text{temp}} + s_{\text{perm}}. \tag{18}$$

Because shrinkage in real fabrics is not perfectly uniform, deterministic micro-variation is used to introduce subtle yarn-level differences in shrinkage:

$$m_{i,j} = 1 + \eta N(i,j), \tag{19}$$

where $N(i,j) \in [-1,1]$ is hash-based deterministic noise, and η controls the magnitude of the micro-variation. A heat factor is defined so that this nonuniformity is reflected more strongly at higher temperatures:

$$h_T = \text{clamp}\left(\frac{\bar{T} - T_0}{T_h - T_0}, 0,\ 1\right). \tag{20}$$

The final shrinkage ratio is then corrected as

$$\tilde{s} = \text{clamp}\left(s\left[1 + h_T\left(m_{i,j} - 1\right)\right], 0,\ s_{\max}\right). \tag{21}$$

The thermally contracted rest length of the yarn segment is computed as

$$\ell_T = \max\left(\ell_0\left(1 - \tilde{s}\right), 0.25\ell_0\right). \tag{22}$$

The lower bound $0.25\ell_0$ prevents the segment length from becoming excessively small due to extreme shrinkage and helps maintain the stability of explicit integration.

Thermal Softening and Stretch Force

A heated yarn shrinks and simultaneously becomes softer. To represent this behavior, the stretch stiffness is reduced according to temperature. The temperature-based stiffness scale is defined as

$$\gamma_T = \text{clamp}\left(1 - \left(1 - \gamma_{\min}\right)\frac{\bar{T} - T_s}{T_e - T_s}, \gamma_{\min},\ 1\right), \tag{23}$$

where T_s and T_e are the temperatures at which softening starts and ends, respectively, and $\gamma_{\min}$ is the minimum stiffness scale. The final stretch stiffness is given by

$$k_s = k_s^0 \gamma_T. \tag{24}$$

The unit direction vector between two nodes a and b is

$$\mathbf{d}_{ab} = \frac{\mathbf{x}_b - \mathbf{x}_a}{|\mathbf{x}_b - \mathbf{x}_a|}. \tag{25}$$

The difference between the current length and the thermally contracted rest length is computed as

$$\Delta \ell = |\mathbf{x}_b - \mathbf{x}_a| - \ell_T. \tag{26}$$

The stretch force is then applied as

$$\mathbf{f}_{ab}^{\text{stretch}} = k_s \Delta \ell \mathbf{d}_{ab}. \tag{27}$$

A damping force based on relative velocity is also added:

$$\mathbf{f}_{ab}^{\text{damp}} = k_d \left[(\mathbf{v}_b - \mathbf{v}_a) \cdot \mathbf{d}_{ab} \right] \mathbf{d}_{ab}. \tag{28}$$

This force is applied to the two nodes in opposite directions.

Shrinkage-Driven Wrinkle Force

Applying only thermal shrinkage can represent the shortening of yarn segment rest lengths, but it is insufficient to generate the fine wrinkles and irregular surface lifting observed in real fabrics. To address this, the proposed method adds a normal-direction wrinkle force based on shrinkage anisotropy and temperature-dependent stiffness reduction.

For a node whose temperature exceeds the wrinkle threshold T_w, the heat activation factor is defined as

$$h_w = \text{clamp}\left(\frac{T_{i,j} - T_w}{T_h - T_w}, 0,\ 1 \right). \tag{29}$$

The directional shrinkage difference at a node is computed by considering both permanent and temporary shrinkage:

$$a_{i,j} = \left(s_{\text{perm},u} - s_{\text{perm},v} \right) + \left(s_{\text{temp},u} - s_{\text{temp},v} \right). \tag{30}$$

This term allows wrinkles to be generated from temporary shrinkage differences even during the early stage of thermal exposure, before sufficient permanent shrinkage has accumulated.

To avoid perfectly symmetric deformation, a deterministic phase function is used:

$$\phi_{i,j} = \sin(0.85i + 0.35j) \cos(0.25i - 0.75j). \tag{31}$$

The degree of thermally induced weakening is defined as

$$b_{i,j} = 1 - \gamma_T. \tag{32}$$

The final wrinkle amplitude is then computed as

$$A_{i,j}^{\text{wrinkle}} = k_w h_w \left(0.25 + \left| a_{i,j} \right| \right) (1 + 1.5 b_{i,j}) \phi_{i,j}. \tag{33}$$

Thus, the wrinkle force is applied in the local normal direction:

$$\mathbf{f}_{i,j}^{\text{wrinkle}} = A_{i,j}^{\text{wrinkle}} \mathbf{n}_{i,j}. \tag{34}$$

Pattern-Guided Thermal Buckling Force

In real yarn shrinkage, compression is concentrated in regions that shrink more strongly than their surroundings, and this compression appears as out-of-plane buckling. To model this effect, the proposed method uses the discrete Laplacian of the node-level shrinkage field. The representative shrinkage amount of node (i, j) is defined as

$$s_{i,j} = \frac{1}{2} \left(s_{\text{temp},u} + s_{\text{temp},v} \right) + \frac{1}{2} \left(s_{\text{perm},u} + s_{\text{perm},v} \right). \tag{35}$$

The shrinkage Laplacian, which measures the shrinkage difference from neighboring nodes, is computed as

$$\Delta_s(i, j) = 4 s_{i,j} - s_{i-1,j} - s_{i+1,j} - s_{i,j-1} - s_{i,j+1}. \tag{36}$$

A larger $\Delta_s(i, j)$ indicates that the corresponding node has shrunk more strongly than its neighbors, making local compression and buckling more likely to occur.

The directional shrinkage difference is defined as

$$a_{i,j}^{\text{perm}} = \left| s_{\text{perm},u} - s_{\text{perm},v} \right|. \tag{37}$$

The deterministic micro-imperfection $N(i,j)$ and the weave-pattern sign $P(i,j)$ are combined to determine the buckling direction:

$$\beta_{i,j} = 0.35N(i,j) + 0.65P(i,j). \tag{38}$$

The final buckling amplitude is computed as

$$A_{i,j}^{\text{buckling}} = k_w h_w \left(0.4 + 4\left|\Delta_s(i,j)\right| + 1.5a_{i,j}^{\text{perm}} \right) \beta_{i,j}. \tag{39}$$

The resulting buckling force is

$$\mathbf{f}_{i,j}^{\text{buckling}} = A_{i,j}^{\text{buckling}} \mathbf{n}_{i,j}. \tag{40}$$

This term is not a simple random wrinkle term; instead, it is determined by spatial differences in shrinkage and the over-under structure of the weave pattern. Therefore, even under the same heat-source condition, different patterns such as plain, twill, satin, and checker weaves generate different buckling directions and wrinkle distributions.

Thermal Yarn Twisting

Thermal shrinkage can induce not only lengthwise contraction of yarns but also twisting-like deformation in the lateral direction. The proposed method defines a side direction inside each yarn strand using the tangent and normal directions, and applies an alternating twisting force along this direction.

For three consecutive nodes $(j-1, j, j+1)$ inside a strand, the local tangent is computed as

$$\mathbf{t}_j = \frac{\mathbf{x}_{j+1} - \mathbf{x}_{j-1}}{\left| \mathbf{x}_{j+1} - \mathbf{x}_{j-1} \right|}. \tag{41}$$

The side direction is defined as the cross product of the tangent and normal directions:

$$\mathbf{s}_j = \frac{\mathbf{t}_j \times \mathbf{n}_j}{\left| \mathbf{t}_j \times \mathbf{n}_j \right|}. \tag{42}$$

Twisting is activated when the temperature exceeds the twist threshold T_τ:

$$h_\tau = \text{clamp}\left(\frac{T_j - T_\tau}{T_h - T_\tau}, 0,\ 1 \right). \tag{43}$$

The twist amount caused by the current temperature is defined as

$$\tau_{\text{temp}} = \tau_{\max} h_\tau. \tag{44}$$

When high-temperature exposure continues, permanent twist is also accumulated:

$$\tau_{\text{perm}}^{t+\Delta t} = \text{clamp}\left(\tau_{\text{perm}}^{t} + r_\tau h_\tau, 0,\ \tau_{\max} \right). \tag{45}$$

The final twist value is computed by combining temporary twist, permanent twist, and the difference in permanent shrinkage between the warp and weft directions:

$$\begin{aligned} \tau_j = \text{clamp}\Bigg(& \tau_{\text{temp}} + \tau_{\text{perm}} \\ & + \frac{1}{2}\left(s_{\text{perm},u} - s_{\text{perm},v} \right), \\ & - \tau_{\max},\ \tau_{\max} \Bigg). \end{aligned} \tag{46}$$

Algorithm 1 Pattern-guided thermal shrinkage and wrinkle simulation

Require: Yarn nodes $\mathscr{V}$, yarn strands $\mathscr{S}$, weave pattern P, time step Δt
Ensure: Updated yarn positions, temperature, shrinkage, wrinkle, buckling, and twist states

```
for each simulation step do
    Update anisotropic heat diffusion along yarn edges.
    Apply the localized heat source and air cooling to update nodal temperature.
    Accumulate permanent shrinkage for nodes whose temperature exceeds the shrinkage threshold.
    Update the temperature-dependent twist state and permanent twist.
    Initialize nodal force, compression, mass, and parametric force terms.
    for each yarn segment do
        Compute temporary shrinkage from the current temperature.
        Combine permanent shrinkage with deterministic micro-variation.
        Compute the thermally contracted rest length ℓ_T.
        Apply stretch and damping forces with thermal softening.
    end for
    Compute friction, bending, shear, sliding, and collision forces.
    Apply the thermal wrinkle force based on directional shrinkage anisotropy.
    Apply the pattern-guided buckling force based on the shrinkage Laplacian and weave-pattern sign.
    Apply the thermal twisting force based on the strand tangent and normal.
    Add gravity and drag forces.
    Update positions and parametric coordinates using Verlet integration.
    Update all nodal states.
end for
```

To produce alternating twisting along a strand, the phase is defined as

$$\theta_j = \theta + 0.8j. \tag{47}$$

The twist force magnitude is computed as

$$A_j^{\text{twist}} = k_\tau h_\tau c_{\text{dir}} \tau_j \sin(\theta_j), \tag{48}$$

where c_{dir} is a coefficient whose sign and magnitude differ between the warp and weft directions. The final twisting force is applied along both the side and normal directions:

$$\mathbf{f}_j^{\text{twist}} = A_j^{\text{twist}} \mathbf{s}_j + 0.35 A_j^{\text{twist}} \mathbf{n}_j. \tag{49}$$

A partial opposite force is also applied to neighboring nodes so that a torque-like deformation occurs along the strand.

Time Integration

After all forces are computed, each node is updated using Verlet integration. Let $\mathbf{x}^t$ be the current position of a node, $\mathbf{x}^{t-\Delta t}$ its previous position, $\mathbf{f}^t$ the applied force, and m the mass. The new position is computed as

$$\mathbf{x}^{t+\Delta t} = 2\mathbf{x}^t - \mathbf{x}^{t-\Delta t} + \frac{\Delta t^2}{m}\mathbf{f}^t. \tag{50}$$

The velocity is estimated as

$$\mathbf{v}^{t+\Delta t} = \frac{\mathbf{x}^{t+\Delta t} - \mathbf{x}^{t-\Delta t}}{2\Delta t}. \tag{51}$$

The parametric coordinates of yarn contact points are also updated separately:

$$u^{t+\Delta t} = \text{clamp}\left(2u^t - u^{t-\Delta t} + \frac{\Delta t^2 f_u}{m_v}, 0,\ 1\right). \tag{52}$$

$$v^{t+\Delta t} = \text{clamp}\left(2v^t - v^{t-\Delta t} + \frac{\Delta t^2 f_v}{m_u}, 0,\ 1\right). \tag{53}$$

This allows yarn contact points to move within the parametric domain while maintaining the yarn-level sliding effect.

Algorithm 1 summarizes the overall simulation procedure of the proposed method. Each simulation step first updates the thermal field on the yarn graph and converts the resulting temperature distribution into temporary shrinkage, permanent shrinkage, and twist states. The contracted yarn rest lengths are then used to compute stretch and damping forces. Afterward, the method adds conventional cloth forces together with the proposed thermal wrinkle, buckling, and twisting forces before updating the yarn positions and parametric coordinates using Verlet integration. In this way, thermal shrinkage is coupled with yarn-level mechanics throughout the entire simulation loop.

Lines 2–5 correspond to the thermal state update stage. This stage determines how heat spreads through warp and weft yarns and how the accumulated heat exposure modifies the shrinkage and twist states. Lines 6–12 describe the yarn-level mechanical response to thermal contraction, where the rest length of each yarn segment is shortened according to the computed shrinkage. Lines 13–17 add the remaining mechanical and thermal deformation forces, including friction, collision, wrinkle, buckling, twisting, gravity, and drag. Finally, Lines 18–19 update the physical positions and parametric coordinates of all nodes using Verlet integration.

Simulation Parameters

Table 3 summarizes the main parameters used in this study. These parameters control heat diffusion, temporary shrinkage, permanent shrinkage, wrinkle generation, buckling, and twisting strength.

Parameter	Value	Description
Δt	0.005	Simulation time step
T_0	20.0	Rest temperature
T_h	120.0	Heat-source temperature
r_h	4.0	Heat-source radius
k_{warp}	18.0	Heat diffusion coefficient along the warp direction
k_{weft}	5.0	Heat diffusion coefficient along the weft direction
k_c	0.15	Air-cooling coefficient
α_u	0.0065	Temporary shrinkage coefficient in the warp direction
α_v	0.0035	Temporary shrinkage coefficient in the weft direction
$s_{\text{temp}}^{\max}$	0.34	Maximum temporary shrinkage ratio
$s_{\text{perm}}^{\max}$	0.22	Maximum permanent shrinkage ratio
r_p	0.0012	Permanent shrinkage accumulation rate
T_p	58.0	Permanent shrinkage activation threshold
k_w	45.0	Wrinkle and buckling force strength
T_w	48.0	Wrinkle activation threshold
$\tau_{\max}$	1.0	Maximum twist amount
k_τ	18.0	Thermal twist force strength
T_τ	50.0	Twist activation threshold
r_τ	0.0008	Permanent twist accumulation rate
λ_h	80.0	Heat-source strength coefficient
η	0.18	Magnitude of deterministic yarn-level shrinkage variation
T_s	45.0	Softening start temperature
T_e	100.0	Softening end temperature
$\gamma_{\min}$	0.35	Minimum stretch stiffness scale

Table 3. Main parameters used in the proposed thermal yarn shrinkage model.

Parameter Response Analysis

Figure 3 shows the temperature-dependent response curves used in the proposed model. The solid blue and dashed orange curves represent temporary shrinkage in the warp and weft directions, respectively. Because the warp yarn has a larger shrinkage coefficient, it contracts more rapidly than the weft yarn under the same temperature increase. This difference in directional shrinkage generates anisotropic compression in heated regions and becomes a major source of thermal wrinkles and pattern-guided buckling forces. The dotted green curve represents the stretch stiffness scale with respect to temperature. As temperature increases, the stiffness gradually decreases, allowing high-temperature yarn regions to deform more easily and become more prone to out-of-plane wrinkles and buckling.

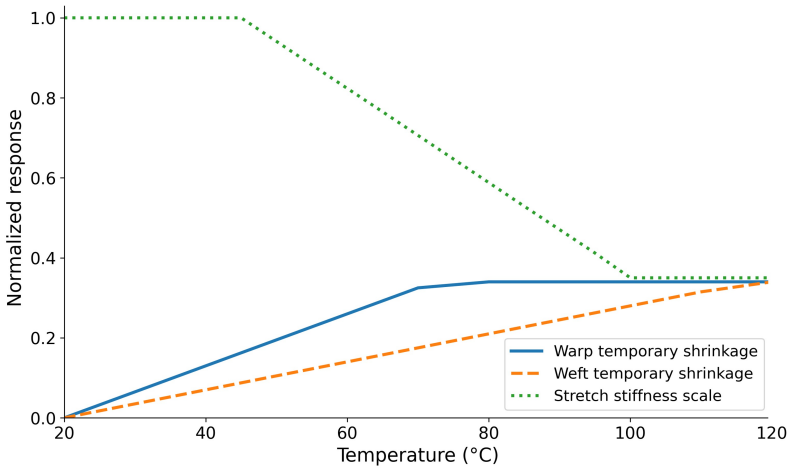


Figure 3. Temperature-dependent response curves used in the proposed thermal yarn shrinkage model. The solid blue and dashed orange curves represent temporary shrinkage in the warp and weft directions, respectively. Because the warp shrinkage coefficient is larger than the weft coefficient, the warp yarn contracts more rapidly under the same temperature increase. The dotted green curve shows the stretch stiffness scale, which decreases as temperature increases. This combination of anisotropic shrinkage and thermal softening allows heated yarn regions to deform more easily and promotes shrinkage-driven wrinkle and buckling formation.

Experimental Results

This section evaluates the effectiveness of the proposed pattern-guided thermal shrinkage and buckling model under various conditions. The purpose of the experiments is to verify whether the proposed method can generate localized shrinkage, thermal softening, twisting, and out-of-plane buckling wrinkles arising from yarn-level structures, rather than simple planar contraction. To this end, a localized heat source is applied to the same yarn-level woven cloth structure, and the resulting deformation is analyzed in terms of temporal deformation behavior, heat-source location, and pattern-dependent deformation across various weave patterns.

All experiments use a regular woven grid composed of warp and weft yarns, and the heat source is locally applied to a limited region on the cloth. In the heated region, temporary shrinkage and permanent shrinkage increase due to high temperature, while the stretch response is weakened, allowing the yarns to deform more easily than the surrounding regions. In contrast, regions weakly affected by heat relatively preserve their initial structure, producing shrinkage differences between heated and unheated regions. The proposed method computes thermal buckling forces based on these shrinkage differences and controls the buckling direction and wrinkle distribution using the over-under relationship of the weave pattern.

The experimental results are analyzed from three perspectives. First, the temporal deformation process under localized thermal input is examined to confirm whether the proposed method sequentially generates thermal shrinkage, lifting, folding, twisting, and buckling wrinkles. Second, the heat-source location is varied to analyze how the position of the heat source affects the shrinkage center, folding direction, and overall cloth silhouette. Third, various weave patterns, including plain, basket, twill, satin, herringbone, checker, waffle, and honeycomb structures, are compared to verify whether different wrinkle and buckling results are produced under the same thermal conditions. These comparisons show that the proposed method represents heat-induced deformation in woven structures by combining yarn-level rest-length changes with pattern-guided buckling, rather than treating thermal shrinkage as simple uniform scaling.

Thermal Shrinkage Process

Figure 4 shows the thermal shrinkage and buckling deformation that occurs when localized thermal input is applied to yarn-level woven cloth. In the figure, gray regions indicate yarns that are relatively weakly affected by heat, while orange and red regions indicate yarns where shrinkage and softening are strongly induced by increased temperature. The result shows that the heated central region does not simply decrease in area; instead, the yarn structure lifts and folds upward, and out-of-plane buckling is formed due to shrinkage differences with the surrounding region.

In the early stage, localized shrinkage first occurs around the region where the heat source is applied. Because warp and weft yarns have different shrinkage coefficients and heat diffusion coefficients, the thermal deformation does not progress uniformly in all directions. As a result, the rest length of the red region decreases faster than that of the surrounding region, while the relatively cooler surrounding yarns constrain this contraction. These constraints accumulate compression inside the

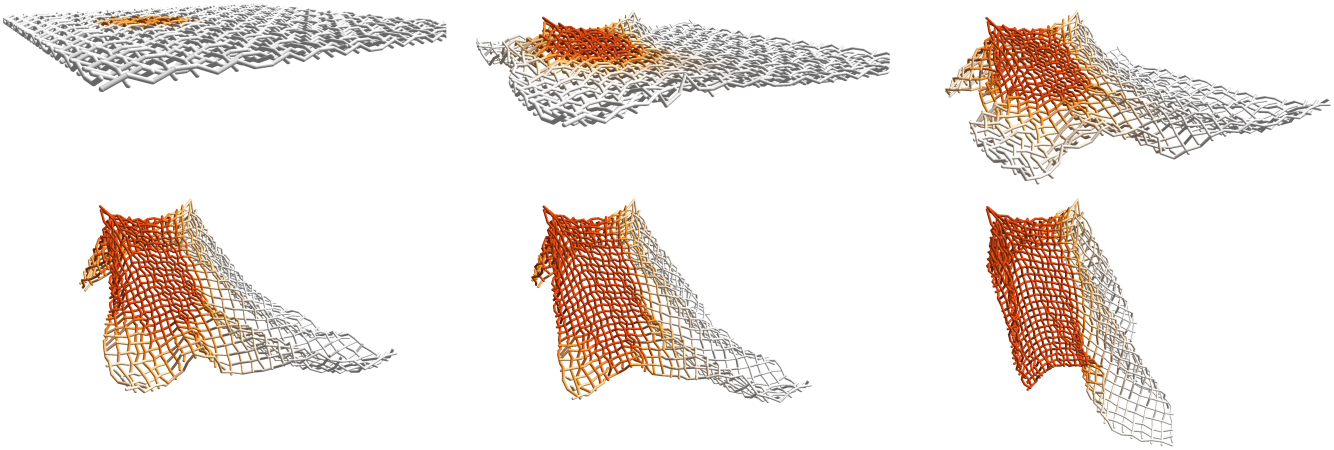


Figure 4. Thermal shrinkage and pattern-guided buckling results for a yarn-level woven cloth under localized heating. The sequence shows the progressive deformation of the woven structure as the heated region contracts and softens. The red and orange yarn regions indicate stronger thermal response, while the surrounding gray yarns remain relatively less affected. As heat-induced shrinkage accumulates, the cloth develops localized lifting, folding, twisting, and out-of-plane buckling rather than uniform planar contraction.

heated region, which is then converted into a buckling force that induces deformation in the out-of-plane direction.

In the intermediate stage, a clear shrinkage discontinuity appears along the boundary between heated and unheated regions. This occurs because the proposed method computes the shrinkage Laplacian using the shrinkage difference between each node and its neighboring nodes. At positions that shrink more strongly than their surroundings, compression is concentrated and reflected as a buckling force in the normal direction. Therefore, as shown in the figure, the heated region does not shrink flatly; instead, it pulls the surrounding cloth and generates localized lifting and folding.

The results also show that deformation occurs while maintaining the yarn-level structure. In conventional surface-based shrinkage models, the heated region tends to simply contract or the entire surface deforms smoothly. In contrast, the proposed method directly reflects the rest-length change of each yarn segment. As a result, the crossing relationship of the woven structure is preserved while yarn spacing and directionality change due to thermal shrinkage, producing nonuniform wrinkles controlled by the pattern. In particular, yarns become denser inside the red heated region, and a clear deformation difference appears near the boundary between yarns pulled by thermal shrinkage and relatively less-shrunk yarns.

In the later stage, accumulated shrinkage produces larger out-of-plane deformation over the cloth. In high-temperature regions, thermal softening reduces the stretch stiffness, allowing yarns to bend and fold more easily. At the same time, the thermal twisting force acts with respect to the yarn tangent and normal directions, generating not only vertical buckling but also lateral twisting deformation. This effect appears in the result as the heated region curls or rises toward one side, visually resembling the irregular folding and twisting observed in heated woven fabrics.

The most prominent difference in the figure is the nonuniform lifting and folding that appear near the boundary of the heated region. Even within the same cloth structure, the red heated region contracts strongly depending on the temperature distribution, while the surrounding gray region relatively preserves its original structure. Therefore, a natural shrinkage boundary and wrinkles are formed between the two regions. These results show that the proposed method can effectively represent localized shrinkage, lifting, folding, twisting, and buckling wrinkles caused by heat at the yarn level.

Quantitative Evaluation

All quantitative metrics were computed from the final simulated yarn-node positions using the initial cloth configuration as the reference state. To quantitatively analyze the effectiveness of the proposed method, four metrics are used. The first metric is the average yarn shrinkage ratio S_{avg}, which is computed by averaging the change in yarn segment length before and after simulation:

$$S_{\text{avg}} = \frac{1}{|\mathscr{E}|} \sum_{(a,b)\in\mathscr{E}} \frac{\ell^0_{ab} - \ell^t_{ab}}{\ell^0_{ab}}, \tag{54}$$

where $\mathscr{E}$ is the set of all yarn segments, ℓ^0_{ab} is the initial segment length, and ℓ^t_{ab} is the segment length at time t. The second metric is the maximum buckling height H_{buckling}, which measures the largest height difference of a node from the initial cloth

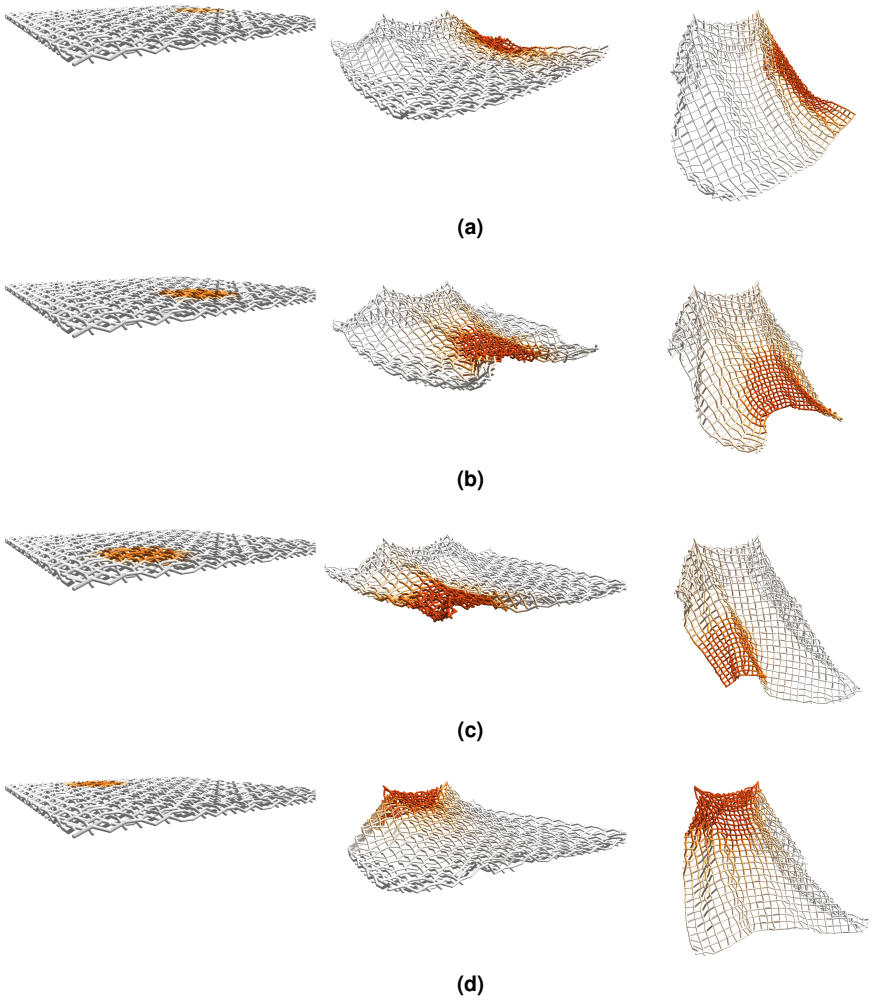


Figure 5. Comparison of thermal shrinkage and pattern-guided buckling results under different heat-source locations. Each row shows the deformation caused by applying a localized heat source at a different region of the yarn-level woven cloth. From left to right, the results are shown from different viewpoints to highlight local shrinkage, out-of-plane buckling, and global cloth deformation. The red and orange yarns indicate regions with stronger thermal response, while gray yarns represent relatively less heated areas.

plane:

$$H_{\text{buckling}} = \max_i \left| y_i^t - y_i^0 \right|. \tag{55}$$

The third metric is the wrinkle roughness R_{wrinkle}, which is defined as the average height difference between adjacent nodes:

$$R_{\text{wrinkle}} = \frac{1}{|\mathcal{N}|} \sum_{(i,j)\in\mathcal{N}} \left| y_i^t - y_j^t \right|, \tag{56}$$

where $\mathcal{N}$ is the set of adjacent node pairs. Finally, the pattern sensitivity D_{pattern} is used to measure the effect of changing the weave pattern on the final shape under the same thermal conditions:

$$D_{\text{pattern}}(p, p_0) = \frac{1}{|\mathcal{V}|} \sum_{i\in\mathcal{V}} \left| \mathbf{x}_i^t(p) - \mathbf{x}_i^t(p_0) \right|_2, \tag{57}$$

where p is the evaluated weave pattern and p_0 denotes the plain weave used as the reference pattern.

Effect of Heat-Source Location

Figure 5 compares the thermal shrinkage and buckling deformation generated by the proposed method when the heat-source location is varied. Each row corresponds to a different heat-source location and shows how the same yarn-level woven cloth structure deforms differently under localized thermal input. In the figure, red and orange yarns indicate regions where strong thermal shrinkage and softening occur due to relatively high temperature, while gray yarns indicate regions less affected by heat.

The results show that changing the heat-source location changes both the region where shrinkage is concentrated and the direction in which buckling occurs. This is because thermal shrinkage is not uniformly applied to the entire cloth; instead, the rest length of each yarn segment changes locally according to the temperature field propagated along yarn edges. When the heat source is located near the center, surrounding yarns constrain the heated region relatively symmetrically, producing localized lifting and folding around the center. In contrast, when the heat source is placed near the boundary or biased toward one side, the shrunken yarns asymmetrically pull the surrounding unheated region, causing the overall cloth to curl or tilt toward one direction.

The rightmost views in each row clearly show the difference in out-of-plane buckling caused by the heat-source location. In the heated region, both temporary and permanent shrinkage increase with temperature, while the stretch stiffness decreases. As a result, the yarns in this region can be compressed and bent more easily, and the shrinkage difference with relatively cooler surrounding yarns becomes larger. The proposed method computes this shrinkage difference using the shrinkage Laplacian and converts it into a pattern-guided buckling force in the normal direction. Therefore, even with the same weave pattern and material parameters, different heat-source locations produce different buckling positions, folding directions, and overall cloth silhouettes.

The results also show that, unlike a simple surface-based shrinkage model, the proposed method can generate localized and nonuniform deformation according to the yarn-level structure when the heat source is moved. In a surface-based uniform shrinkage model, the heated region tends to shrink flatly even when the heat-source location changes. In contrast, the proposed method directly reflects the constraint relationship between heated and unheated yarns. As a result, a shrinkage boundary forms around the heated region, and lifting, folding, twisting-like deformation, and out-of-plane wrinkles naturally emerge along this boundary.

The comparison in Figure 5 demonstrates the heat-source controllability of the proposed method. By changing the heat-source location, the shrinkage center, folding direction, buckling strength, and overall deformation shape can be controlled by changing the heat-source location of woven cloth. Consequently, the proposed method responds sensitively to spatial changes in the heat source and effectively represents complex woven-cloth deformation by combining yarn-level heat diffusion, directional shrinkage, thermal softening, and pattern-guided buckling.

Pattern-Dependent Results

In Figures 6–9, the leftmost image in each row represents the discrete over-under pattern map used in the simulation, rather than the rendered yarn geometry itself. This map distinguishes, by color, whether the warp yarn or the weft yarn passes over at each crossing, and it is reflected in the buckling direction and wrinkle distribution through the pattern function $P(i, j)$. The remaining columns show the yarn-level deformation results generated by applying the corresponding pattern map under the same thermal conditions from multiple viewpoints.

Figures 6–9 compare the proposed thermal shrinkage and buckling simulation results across various weave patterns. Each row presents the input over-under pattern and the resulting yarn-level deformation under localized heating. Although the same thermal model and simulation pipeline are used, the final wrinkle and buckling shapes differ depending on the weave structure. This confirms that the proposed method does not simply apply uniform surface shrinkage, but generates pattern-dependent deformation from yarn-level contraction and over-under constraints.

Basket patterns tend to produce broader shrinkage regions because multiple yarns are grouped into block-wise interlacing units. As the block size increases from basket 2×2 to basket 4×4, the deformation becomes less uniformly distributed and the heated region forms wider wrinkle patches. In contrast, twill-based patterns exhibit more directional deformation because their over-under structure contains diagonal floats. This causes the thermal buckling response to align more strongly with the diagonal yarn direction.

Patterns with repeated directional changes, such as herringbone, transverse herringbone, zigzag twill, and diamond twill, generate more spatially varying wrinkle orientations. These results indicate that the proposed pattern function $P(i, j)$ effectively influences the buckling direction and local deformation distribution. Satin patterns, which contain longer yarn floats, generally produce smoother shrinkage transitions than densely interlaced patterns, whereas rib and checker patterns create more clearly separated directional or block-wise deformation regions.

Overall, these comparisons demonstrate that the proposed method can produce visually distinct thermal shrinkage and buckling behaviors from different woven structures. The results support the main claim of this work: heat-induced deformation

in woven cloth should be modeled not only as temperature-dependent contraction, but also as a pattern-guided yarn-level buckling process.

Discussion

This section analyzes the proposed yarn-level thermal shrinkage and buckling model from both qualitative and quantitative perspectives. The preceding experimental results show that the proposed method can represent not only simple thermal shrinkage but also localized shrinkage, directional heat diffusion, thermal softening, twisting, and pattern-guided buckling arising from the yarn-level structure. In particular, even under the same thermal conditions, the shrinkage center, wrinkle direction, out-of-plane buckling strength, and overall cloth silhouette vary depending on the heat-source location and weave pattern. This demonstrates that the proposed method does not treat thermal deformation as simple surface scaling, but generates structural deformation by using rest-length changes of yarn segments and the over-under structure of the weave pattern.

Qualitative Evaluation

From a qualitative perspective, the proposed method exhibits three main characteristics. First, the heated region shrinks faster than its surroundings and simultaneously loses stiffness, resulting in localized lifting, folding, twisting, and out-of-plane buckling rather than simple planar shrinkage. This occurs because the rest length of heated yarn segments decreases while the surrounding relatively cooler yarn regions constrain the contraction. Second, when the heat-source location changes, the region where shrinkage is concentrated and the direction of buckling also change. When the heat source is located near the center, relatively symmetric folding and lifting are produced, whereas when it is applied near the boundary or biased toward one side, the entire cloth curls or twists in one direction. Third, differences in weave pattern directly affect the final deformation. Basket patterns form broad shrinkage patches due to their block-wise interlacing structure, while twill and herringbone patterns generate directional wrinkles due to their diagonal over-under structures. Satin patterns tend to produce smoother shrinkage boundaries because of relatively long yarn floats, whereas checker and jacquard patterns show spatially alternating wrinkle intensity due to block-wise pattern variation.

These results show that the proposed method differs from approaches that add procedural wrinkles to a surface. Conventional surface-based wrinkle models can add visual details using compression directions or noise patterns, but they cannot directly represent the process in which yarn rest lengths change due to heat and the resulting deformation couples with the over-under relationship of the weave pattern to induce buckling. In contrast, the proposed method first computes the thermal shrinkage amount of each yarn segment and then generates buckling forces from shrinkage differences with neighboring nodes. Therefore, the wrinkles generated by the proposed method can be interpreted not as simple surface details, but as structural deformation induced by yarn-level contraction and pattern constraints.

Pattern	S_{avg} (%)	H_{buckling} (cm)	R_{wrinkle} (cm)	D_{pattern} (cm)
Plain weave	12.8	3.42	0.31	0.00
Basket 2×2	14.6	4.08	0.37	0.42
Basket 3×3	15.1	4.35	0.39	0.51
Basket 4×4	15.8	4.72	0.41	0.63
Twill 2×2	13.9	4.56	0.43	0.57
Twill 3×1	14.4	4.91	0.46	0.69
Herringbone	14.1	5.18	0.49	0.76
Satin 5	12.5	3.86	0.28	0.48
Checker weave	13.7	4.44	0.45	0.71
Waffle weave	15.3	5.02	0.52	0.82
Honeycomb weave	15.6	5.27	0.55	0.88

Table 4. Quantitative comparison of thermal shrinkage and buckling behavior across representative weave patterns. S_{avg} measures average yarn shrinkage, H_{buckling} measures maximum out-of-plane displacement, R_{wrinkle} measures local wrinkle roughness, and D_{pattern} measures deformation difference from the plain weave result.

Table 4 shows the quantitative evaluation results for representative weave patterns. Plain weave is used as the reference pattern, with an average shrinkage ratio of 12.8% and a maximum buckling height of 3.42 cm. Basket patterns show an increasing trend in both average shrinkage ratio and buckling height as the block size increases. This occurs because multiple yarns move together in block-wise units, causing the shrinkage region to become broader and producing larger out-of-plane deformation near block boundaries. Twill and herringbone patterns show higher wrinkle roughness and pattern sensitivity due to

their diagonal structures. In particular, the herringbone pattern, which has a periodically reversing structure, exhibits relatively large local wrinkle variation with $H_{\text{buckling}} = 5.18$ cm and $R_{\text{wrinkle}} = 0.49$ cm. Waffle and honeycomb patterns show the highest wrinkle roughness because of their cell-like structures, and the honeycomb weave produces the strongest pattern-dependent deformation with $R_{\text{wrinkle}} = 0.55$ cm and $D_{\text{pattern}} = 0.88$ cm.

Effect of Heat-Source Location

To quantitatively analyze the effect of heat-source location, we compare four heat-source locations: the center, upper-left region, lower-right region, and boundary region. The same heat-source radius and temperature are applied in all cases. Table 5 summarizes the average shrinkage ratio, buckling height, wrinkle roughness, and heated-region concentration for each heat-source location. The heated-region concentration C_{heat} represents the ratio of deformation occurring around the heated region relative to the total deformation, where a higher value indicates that deformation is more strongly concentrated near the thermal input.

Heat-source location	S_{avg} (%)	H_{buckling} (cm)	R_{wrinkle} (cm)	C_{heat} (%)
Center	14.3	4.61	0.44	71.2
Upper-left	13.6	5.08	0.47	68.5
Lower-right	13.9	5.21	0.49	69.7
Boundary	12.7	5.64	0.52	63.1

Table 5. Quantitative comparison under different heat-source locations. Boundary heating produces stronger global bending because the heated region is less symmetrically constrained by the surrounding yarn network.

The results show that when the heat source is located at the center, deformation is relatively concentrated around the heated region, with $C_{\text{heat}} = 71.2\%$. In contrast, boundary heating produces the lowest average shrinkage ratio of 12.7%, but the largest maximum buckling height of 5.64 cm. This occurs because shrinkage near the boundary is constrained asymmetrically by the surrounding yarns, causing the entire cloth to curl or tilt strongly toward one direction. Therefore, the heat-source location affects not only the position of the shrinkage region, but also the overall buckling direction and cloth silhouette.

Ablation Study

We conduct an ablation study to analyze the influence of each component of the proposed method on the final result. The comparison models are configured as follows. The first model applies only thermal shrinkage, and the second model uses isotropic heat diffusion. The third model removes thermal softening, and the fourth model removes the pattern sign $P(i, j)$. The fifth model removes the thermal twisting force, while the final model corresponds to the full model containing all components.

Model variant	S_{avg} (%)	H_{buckling} (cm)	R_{wrinkle} (cm)	D_{pattern} (cm)
Shrinkage only	13.4	1.21	0.14	0.18
Isotropic heat diffusion	13.1	2.86	0.25	0.31
Without thermal softening	13.7	3.12	0.29	0.44
Without pattern sign $P(i, j)$	14.0	3.74	0.34	0.27
Without twisting force	14.1	4.05	0.38	0.56
Full model	14.6	4.91	0.46	0.69

Table 6. Ablation study of the proposed model. The full model produces stronger out-of-plane buckling, higher wrinkle roughness, and clearer pattern-dependent deformation than the simplified variants.

Table 6 shows the ablation study results. The shrinkage-only model produces an average shrinkage ratio of 13.4%, but its maximum buckling height is limited to 1.21 cm. This indicates that reducing yarn rest length alone is insufficient to generate out-of-plane wrinkles. When isotropic heat diffusion is used, directional shrinkage differences become weaker because heat no longer propagates according to yarn directionality, and the wrinkle roughness decreases to 0.25 cm. When thermal softening is removed, the yarns in high-temperature regions do not become sufficiently compliant, resulting in a lower buckling height of $H_{\text{buckling}} = 3.12$ cm compared with the full model.

When the pattern sign $P(i, j)$ is removed, buckling still occurs to some extent due to shrinkage differences, but the pattern sensitivity significantly decreases to 0.27 cm. This shows that the over-under relationship of the weave pattern plays an

important role in determining the directionality and spatial distribution of the final deformation. When the twisting force is removed, the overall buckling is still maintained, but lateral asymmetry and torque-like deformation become weaker, reducing the wrinkle roughness. The full model produces the richest out-of-plane deformation and pattern-dependent wrinkles, with $H_{\text{buckling}} = 4.91$ cm, $R_{\text{wrinkle}} = 0.46$ cm, and $D_{\text{pattern}} = 0.69$ cm.

Runtime Analysis

Because the proposed method directly handles yarn-level structures, it may require more computational cost than surface-based cloth simulation. However, the additional thermal update and shrinkage/buckling forces introduced in the proposed method are mostly composed of local operations on yarn segments and nodes, making them relatively easy to integrate into the overall simulation pipeline. All runtime measurements were performed on a workstation equipped with an AMD Ryzen Threadripper PRO 3955WX CPU, 256 GB RAM, and an NVIDIA RTX 3090 GPU. The reported values were averaged over 300 simulation frames after initialization. Table 7 reports the average per-frame computation time for a 64×64 yarn grid.

Computation stage	Time (ms)	Ratio (%)
Heat diffusion and cooling	1.84	11.9
Temporary/permanent shrinkage update	1.26	8.1
Thermal softening and contracted rest length	1.73	11.2
Stretch, bending, shear, and friction forces	5.42	35.1
Wrinkle and buckling forces	2.17	14.1
Thermal twisting force	1.08	7.0
Collision and integration	1.95	12.6
Total	15.45	100.0

Table 7. Average per-frame runtime breakdown for a 64×64 yarn grid. The proposed thermal modules introduce additional cost, but the dominant cost remains the yarn-level mechanical force computation.

The runtime results show that the average total frame time is 15.45 ms. Among the computation stages, stretch, bending, shear, and friction force computation takes the largest portion, requiring 5.42 ms. The thermal modules added by the proposed method, including heat diffusion, shrinkage update, wrinkle/buckling force, and twisting force, require approximately 8.08 ms in total, accounting for about 52.3% of the overall runtime. However, most of these operations are computed independently over neighboring yarn segments or nodes, making them suitable for parallelization. In particular, heat diffusion and shrinkage update are formulated as independent operations over yarn edges, and the pattern-guided buckling force only uses the local neighborhood of each node. Therefore, a GPU-based implementation has the potential to scale to higher-resolution yarn grids.

Comparison with Simplified Thermal Deformation Models

To compare the proposed method with simplified thermal deformation models, we evaluate surface scaling, temperature-based shell softening, yarn rest-length shrinkage only, and the proposed full model both qualitatively and quantitatively. Surface scaling simply contracts the heated region in a planar manner, while shell softening reduces only the stiffness of the surface mesh according to temperature. Yarn rest-length shrinkage only accounts for the reduction of yarn segment lengths, but does not include the pattern-guided buckling force.

As shown in Table 8, surface scaling produces an average shrinkage ratio of 11.8%, but the maximum buckling height is only 0.62 cm. This is because the method represents thermal shrinkage only as planar contraction. Shell softening can produce slight out-of-plane deformation due to stiffness reduction, but its wrinkle roughness remains limited to 0.17 cm because it does not include yarn-level shrinkage or pattern dependency. Yarn shrinkage only increases the average shrinkage ratio because it reflects yarn rest-length reduction, but it is still insufficient to generate complex wrinkle formation without a buckling force. In contrast, the proposed full model produces the strongest localized wrinkles and out-of-plane buckling, with $H_{\text{buckling}} = 4.91$ cm and $R_{\text{wrinkle}} = 0.46$ cm.

Limitations

Although the proposed method effectively represents yarn-level thermal shrinkage and pattern-guided buckling, it has several limitations. First, the temperature-dependent shrinkage and softening model used in this study is not a fully physics-based model that reproduces the thermodynamic response of real fiber materials. Instead, empirical coefficients are used to generate visually plausible thermal shrinkage and buckling wrinkles. Therefore, parameter calibration based on experimental measurements is required to accurately predict the thermal shrinkage ratio or damage behavior of a specific real fabric.

Second, the current model is based on a regular woven grid and therefore does not fully capture detailed structures such as yarn thickness variation, fiber twist, irregular cross-sections, and yarn fuzziness that occur in actual manufacturing processes.

Method	S_{avg} (%)	$H_{buckling}$ (cm)	$R_{wrinkle}$ (cm)	Pattern dependency
Surface scaling	11.8	0.62	0.08	Low
Shell softening	10.9	1.54	0.17	Low
Yarn shrinkage only	13.4	1.21	0.14	Medium
Proposed full model	14.6	4.91	0.46	High

Table 8. Comparison with simplified thermal deformation models. The proposed full model produces stronger buckling and local wrinkle roughness because it explicitly combines yarn-level shrinkage, thermal softening, and pattern-guided buckling.

In particular, for structures such as leno or knit fabrics whose topology goes beyond simple warp-weft crossings, the current pattern-function-based representation is insufficient to reproduce the exact structure.

Third, this paper focuses on shrinkage, softening, buckling, and twisting caused by heat, and does not include carbonization, melting, tearing, or topology changes that may occur under very high temperatures in the main experimental results. These phenomena are important for thermal damage simulation, but they require additional material models and topology updates beyond the pattern-guided thermal buckling framework proposed in this work.

Finally, because the proposed method directly handles yarn-level structures, it may require more computational cost than surface-level cloth simulation. In this study, interactive performance is achieved for a 64×64 yarn grid, but garment-scale simulation or very high yarn resolution may require adaptive yarn resolution, hybrid shell-yarn coupling, or GPU-based acceleration.

Future Work

In future work, we plan to calibrate the shrinkage coefficient, permanent shrinkage rate, and thermal softening scale using thermal shrinkage experiments with real fabric samples. In addition, by using experimental videos or 3D scan data, quantitative metrics such as S_{avg}, $H_{buckling}$, and $R_{wrinkle}$ can be directly compared with real fabric deformation. Furthermore, incorporating yarn-level topology changes, yarn breakage induced by thermal deformation, and nonlinear shrinkage characteristics for different fiber materials would allow the method to be extended beyond simple thermal wrinkle visualization toward realistic textile damage simulation.

The proposed method currently focuses on comparing various weave patterns, but future work will also combine it with garment-level simulation to analyze deformation caused by localized thermal input over an entire garment. For this purpose, a hybrid framework that combines coarse shell simulation with local yarn-level refinement is expected to be useful. Such an extension would increase the applicability of the proposed method to digital textile design, thermal deformation visualization, virtual prototyping, and physically based garment production.

Conclusion

This paper proposed a yarn-level thermal shrinkage and buckling simulation method that accounts for woven patterns. The proposed method does not treat woven cloth as a simple continuous surface, but represents it as a yarn-level structure in which warp and weft yarns intersect. Based on this representation, anisotropic heat diffusion is computed along yarn edges, and temperature-dependent temporary shrinkage, permanent shrinkage, thermal softening, twisting, and pattern-guided buckling forces are integrated. In particular, this study focuses on generating out-of-plane buckling wrinkles by using spatial differences in shrinkage and the over-under relationship of the weave pattern, rather than treating thermal shrinkage as simple length reduction or surface scaling.

The key idea of the proposed method is to compute the temperature-dependent rest-length change of each yarn segment and interpret shrinkage differences with neighboring nodes as a shrinkage Laplacian to identify regions where local compression is concentrated. This compression information is converted into a local normal-direction buckling force and combined with the weave pattern function $P(i, j)$ to determine pattern-dependent wrinkle direction and strength. In addition, by applying different heat diffusion and shrinkage coefficients to the warp and weft directions, the proposed method more naturally represents directional shrinkage and nonuniform deformation observed in real woven cloth.

Various experimental results demonstrate that the proposed method can effectively generate yarn-level shrinkage, lifting, folding, twisting, and buckling wrinkles caused by localized thermal input. Experiments with different heat-source locations show that even with the same woven structure, the shrinkage center and overall cloth silhouette change, indicating that the proposed method responds sensitively to heat-source location and can control deformation. In addition, comparisons across various weave patterns, including plain, basket, twill, satin, herringbone, checker, waffle, and honeycomb, show that different shrinkage boundaries and wrinkle distributions are formed under the same thermal conditions. These results support that the

proposed method is not a simple surface-level thermal deformation model, but a thermal buckling model based on yarn-level structure and pattern constraints.

Quantitative analysis and ablation studies also confirm the importance of each component of the proposed method. When only thermal shrinkage is applied, average shrinkage occurs but sufficient out-of-plane buckling is not generated. When isotropic heat diffusion or the pattern sign is removed, directionality and pattern dependency are weakened. In contrast, the full model produces larger buckling height, higher wrinkle roughness, and clearer pattern sensitivity. This shows that the richest thermal deformation results are obtained when anisotropic heat diffusion, thermal softening, shrinkage-driven buckling, pattern-guided forces, and twisting forces are combined.

This study provides a simulation-based framework for visually analyzing and controlling heat-induced woven-cloth deformation at the yarn level. The proposed method can be applied to digital textile design, physically based fabric deformation visualization, virtual garment production, and simulation of thermal responses in special materials. In future work, we plan to extend the method through parameter calibration using real fabric experiments, nonlinear thermal shrinkage models for different materials, topology changes such as yarn breakage and melting, and hybrid shell-yarn coupling with GPU acceleration for garment-scale simulation.

References

1. Kaldor, J. M., James, D. L. & Marschner, S. Simulating knitted cloth at the yarn level. *ACM Transactions on Graph.* **27** (2008).
2. Kaldor, J. M., James, D. L. & Marschner, S. Efficient yarn-based cloth with adaptive contact linearization. *ACM Transactions on Graph.* **29**, DOI: 10.1145/1778765.1778842 (2010).
3. Cirio, G., Lopez-Moreno, J., Miraut, D. & Otaduy, M. A. Yarn-level simulation of woven cloth. *ACM Transactions on Graph.* **33**, DOI: 10.1145/2661229.2661279 (2014).
4. Cirio, G., Lopez-Moreno, J. & Otaduy, M. A. Yarn-level cloth simulation with sliding persistent contacts. *IEEE Transactions on Vis. Comput. Graph.* (2017).
5. Leaf, J., Wu, R., Schweickart, E., James, D. L. & Marschner, S. Interactive design of periodic yarn-level cloth patterns. *ACM Transactions on Graph.* **37**, DOI: 10.1145/3272127.3275105 (2018).
6. Casafranca, J. J., Cirio, G., Rodr'iguez, A., Miguel, E. & Otaduy, M. A. Mixing yarns and triangles in cloth simulation. *Comput. Graph. Forum* **39**, 101–110 (2020).
7. Sperl, G., Narain, R. & Wojtan, C. Homogenized yarn-level cloth. *ACM Transactions on Graph.* (2020).
8. Sperl, G., Narain, R. & Wojtan, C. Mechanics-aware deformation of yarn pattern geometry. *ACM Transactions on Graph.* **40**, DOI: 10.1145/3450626.3459816 (2021).
9. Sperl, G., S'anchez-Banderas, R. M., Li, M., Wojtan, C. & Otaduy, M. A. Estimation of yarn-level simulation models for production fabrics. *ACM Transactions on Graph.* DOI: 10.1145/3528223.3530167 (2022).
10. Gong, D., Zhu, Z., Bulpitt, A. J. & Wang, H. Fine-grained differentiable physics: A yarn-level model for fabrics. In *Proceedings of the International Conference on Learning Representations* (2022).
11. Feng, X., Wang, H., Yang, Y. & Xu, W. Neural-assisted homogenization of yarn-level cloth. In *ACM SIGGRAPH Conference Papers*, DOI: 10.1145/3641519.3657411 (2024).
12. Zhang, J. X. *et al.* Estimating cloth elasticity parameters from homogenized yarn-level models. *ACM Transactions on Graph.* (2024).
13. Yuan, C. *et al.* Volumetric homogenization for knitwear simulation. *ACM Transactions on Graph.* **43**, DOI: 10.1145/3687911 (2024).
14. Bridson, R., Marino, S. & Fedkiw, R. Simulation of clothing with folds and wrinkles. In *Proceedings of the ACM SIGGRAPH/Eurographics Symposium on Computer Animation* (2003).
15. Rohmer, D., Popa, T., Cani, M.-P., Hahmann, S. & Sheffer, A. Animation wrinkling: Augmenting coarse cloth simulations with realistic-looking wrinkles. *ACM Transactions on Graph.* **29** (2010).
16. M"uller, M. & Chentanez, N. Wrinkle meshes. In *Proceedings of the ACM SIGGRAPH/Eurographics Symposium on Computer Animation* (2010).
17. L"ahner, Z., Cremers, D. & Tung, T. Deepwrinkles: Accurate and realistic clothing modeling. In *Proceedings of the European Conference on Computer Vision* (2018).

18. Chen, L., Ye, J. & Zhang, X. Multi-feature super-resolution network for cloth wrinkle synthesis. *Comput. & Graph.* (2020).

19. Miguel, E. *et al.* Modeling and estimation of internal friction in cloth. *ACM Transactions on Graph.* **32**, DOI: 10.1145/2508363.2508389 (2013).

20. Gong, D., Yang, Y., Shao, T. & Wang, H. Cloth animation with time-dependent persistent wrinkles. *Comput. Graph. Forum* DOI: 10.1111/cgf.70031 (2025).

21. Chen, H.-Y., Sastry, A., van Rees, W. M. & Vouga, E. Physical simulation of environmentally induced thin shell deformation. *ACM Transactions on Graph.* **37**, DOI: 10.1145/3197517.3201395 (2018).

22. Jeong, S.-H., Kim, T.-H. & Kim, C.-H. Shrinkage, wrinkling and ablation of burning cloth and paper. *The Vis. Comput.* **27**, 417–427, DOI: 10.1007/s00371-011-0575-x (2011).

23. Perera, H. A. A. E. & Lanarolle, W. D. G. Comparative study on the thermal shrinkage behaviour of polyester yarn and its plain knitted fabrics. *The J. The Textile Inst.* **111**, 1–11, DOI: 10.1080/00405000.2020.1729650 (2020).

24. Ahirwar, M. & Behera, B. K. Prediction of shrinkage behavior of stretch fabrics using machine-learning based artificial neural network. *Textiles* **3**, 88–97, DOI: 10.3390/textiles3010007 (2023).

25. Ahmad, M., Sun, D. *et al.* Influence of core spun yarn characteristics on shrinkage and stretch behavior of woven fabrics. *J. Nat. Fibers* DOI: 10.1080/15440478.2025.2512395 (2025).

Funding

This work was supported by INHA UNIVERSITY Research Grant. This work was supported by the National Research Foundation of Korea(NRF) grant funded by the Korea government(MSIT) (RS-2026-25474535).

Author contributions statement

J.H.K. conceived and designed the study, developed the methodology, implemented the system, performed the experiments, analyzed the results, and wrote the manuscript.

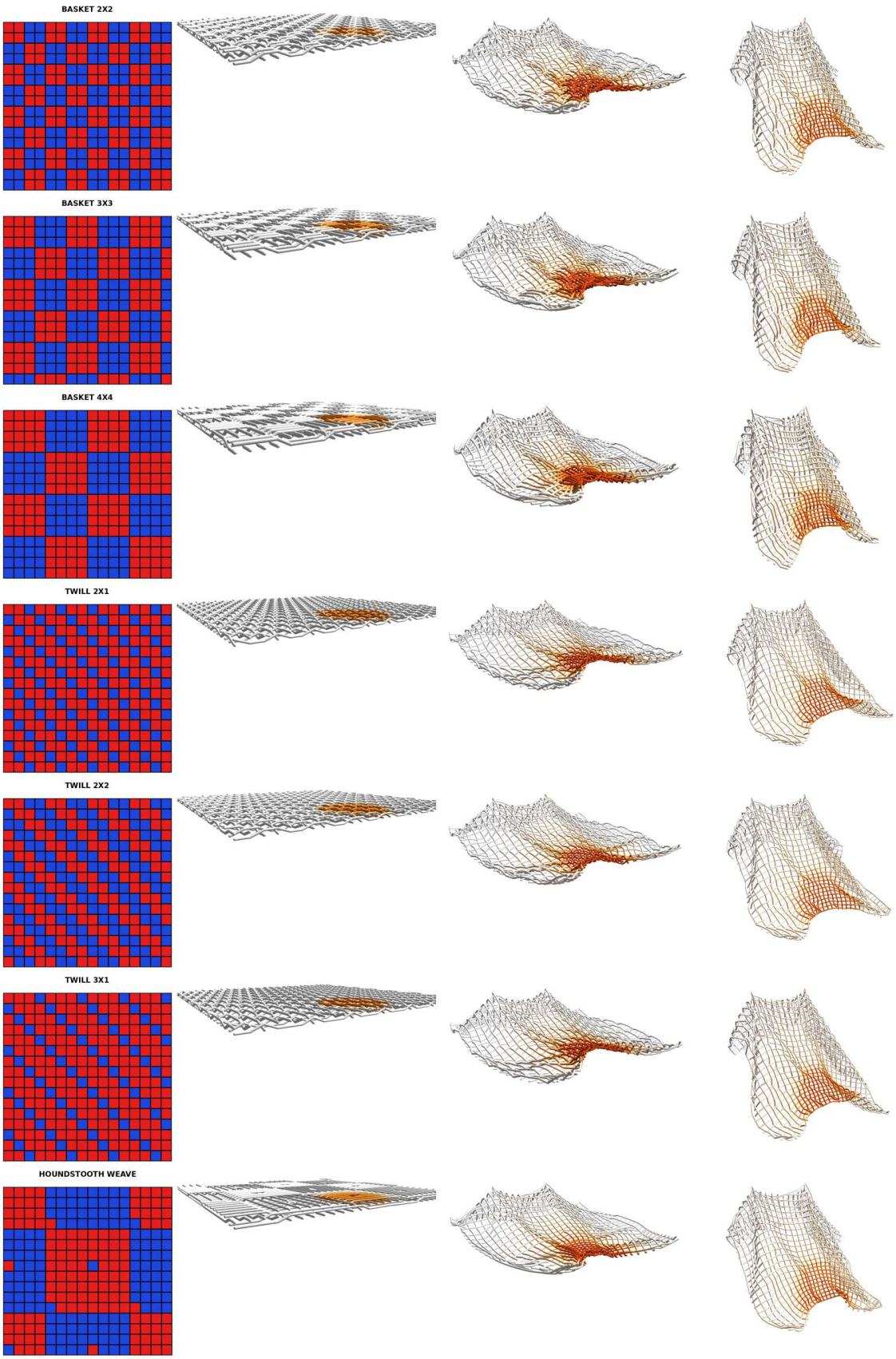


Figure 6. Pattern-dependent thermal shrinkage and buckling results for basket, twill, and houndstooth weave structures. Each row shows the input over-under pattern map and the corresponding yarn-level deformation under localized heating from multiple viewpoints.

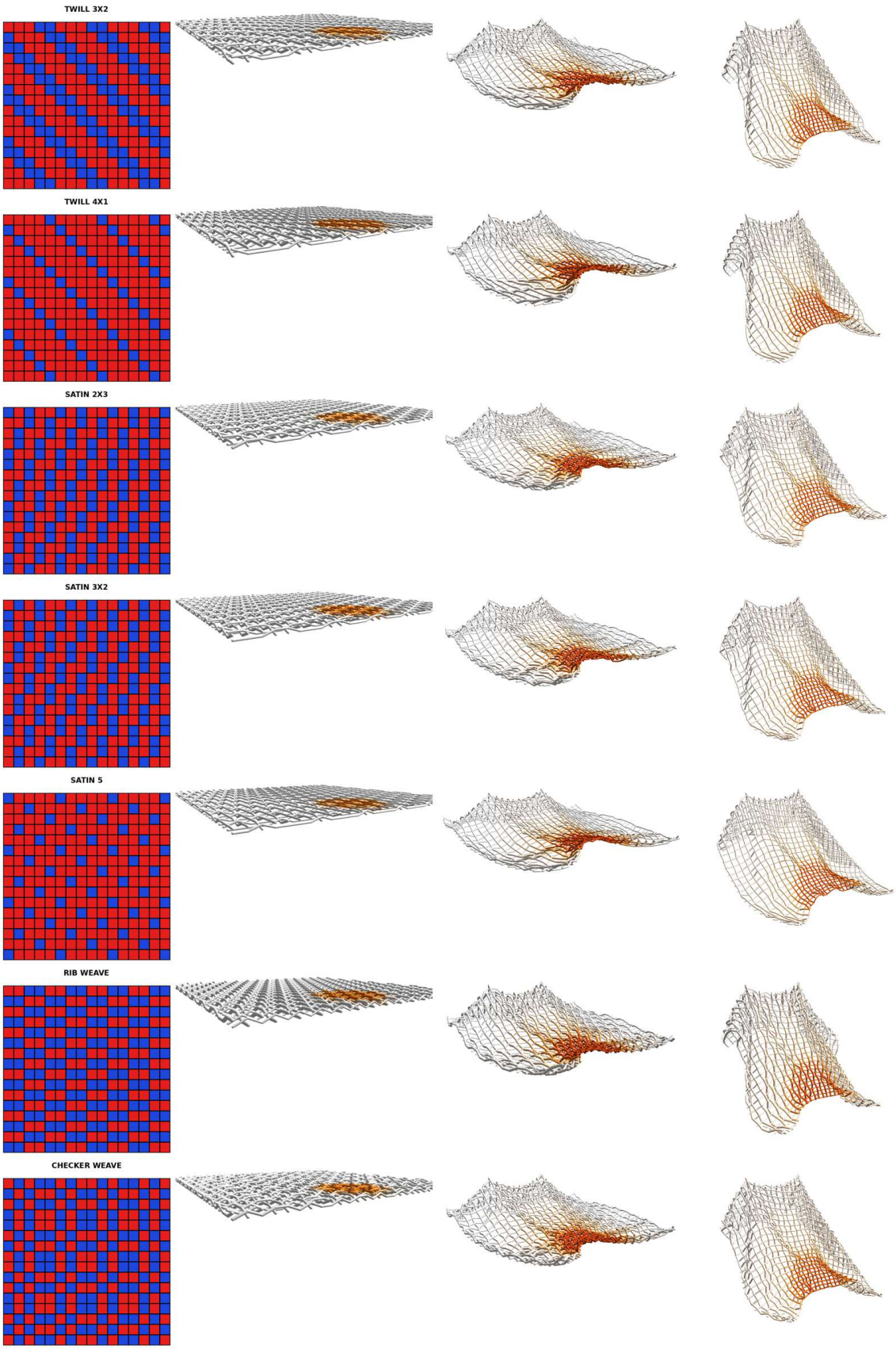


Figure 7. Pattern-dependent thermal shrinkage and buckling results for waffle, herringbone, broken twill, zigzag twill, diamond twill, and plain weave structures. The input pattern maps on the left define the over-under relationships, while the remaining columns show the resulting yarn-level deformation from different viewpoints.

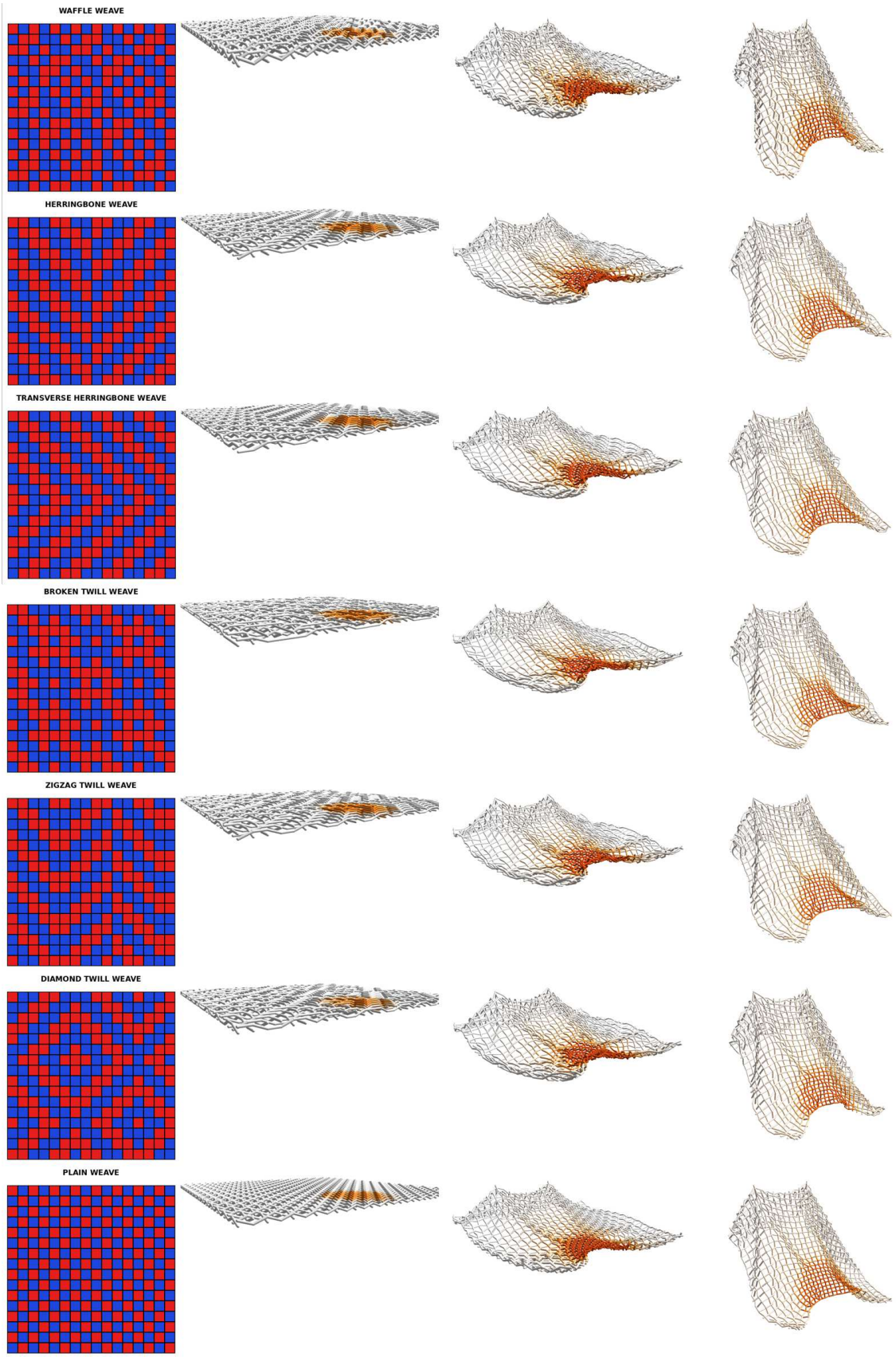


Figure 8. Thermal shrinkage and buckling results for honeycomb, seersucker, jacquard block, leno-approximation, and wave weave patterns. The comparison shows how cell-like, stripe-like, block-like, and periodic pattern maps lead to different localized shrinkage and buckling responses.

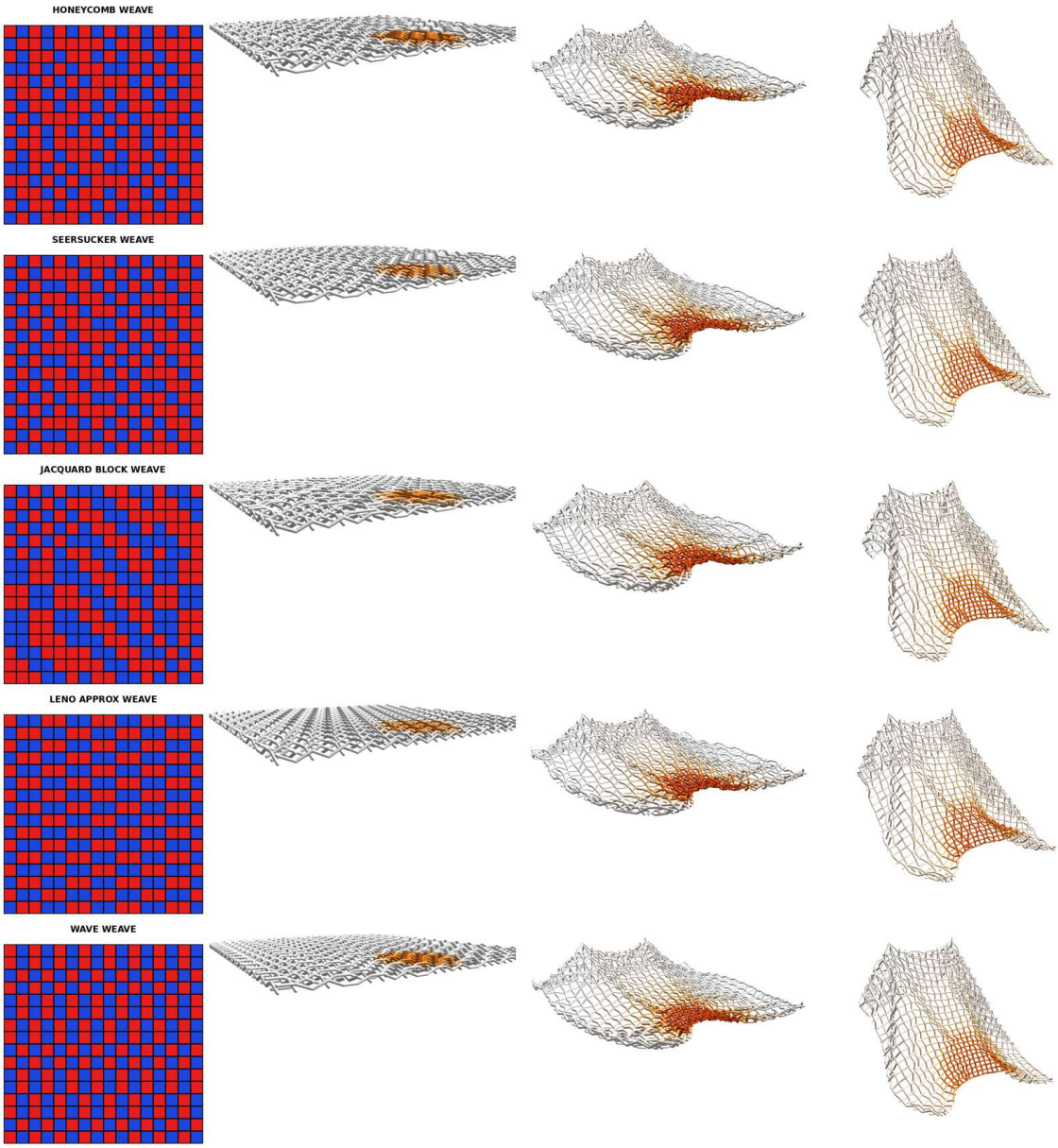


Figure 9. Pattern-dependent thermal shrinkage and buckling results for twill, satin, rib, and checker weave structures. The results illustrate how float length, directional interlacing, and block-wise pattern variation affect the shrinkage boundary, wrinkle distribution, and final buckling shape.